Development of a microfluidic device to produce asymmetric biomimetic liposomes

Auteur : Gilliard, Guillaume
Promoteur(s) : Deleu, Magali; Gilet, Tristan
Faculté : Gembloux Agro-Bio Tech (GxABT)
Diplôme : Master en bioingénieur : chimie et bioindustries, à finalité spécialisée
Année académique : 2018-2019
URI/URL : http://hdl.handle.net/2268.2/8304

LIÈGE université
Gembloux
Agro-Bio Tech

Development of a microfluidic device to produce asymmetric biomimetic liposomes

Guillaume Gilliard

Travail de fin d'études présenté en vue de l'obtention du diplôme de
Master bioingénieur en Chimie et bio-industries

Année académique 2018-2019

(Co)-promoteur(s): Magali Deleu, Tristan Gilet

Acknowledgments / Remerciements

Je tenais tout d'abord à remercier mes deux co-promoteurs de l'Université de Liège, Dr. Magali Deleu du Laboratoire de Biophysique Moléculaire aux Interfaces (LBMI) de la faculté de Gembloux Agro Bio-Tech et Pr. Tristan Gilet du Microfluidics Lab de la faculté des sciences appliquées. Ils m'ont tous deux apporté une aide précieuse et m'ont ré-aiguillé et conseillé tout au long de la rédaction de ce mémoire quand ils le jugeaient nécessaire.

Je désire aussi remercier Stéphanie Van Loo, qui m'a guidé lors de mes premiers pas avec la microfluidique, ainsi que les autres membres du Microfluidics Lab, Loïc Tadrist et Justine Parmentier pour l'accueil chaleureux dont ils m'ont fait part.

Enfin, je dois exprimer ma profonde reconnaissance envers mes parents et ma sœur qui m'ont suivi et soutenu tout au long de mes études au sein de cette belle faculté de Gembloux. C'est aussi grâce à eux si j'ai pu arriver jusqu'ici.

Abstract

The plasma membrane is a complex structure that plays a key role in the function of the cell and some proteins and also in the recognition of “allogenic” molecules. In plants, this structure, and more particularly its lipid fraction, is thought to be involved in the perception of elicitors such as surfactin, a molecule representing a potential alternative to conventional pesticides.

However, the development of such alternatives requires understanding the biological mechanisms at the molecular level. As the plant plasma membrane is a very intricate structure with a huge molecular diversity, simplified biomimetic models such as liposomes have been developed to decipher the molecular mechanisms at stake.

Still, to be correlated with the biological phenomena, these simplified biomimetic models have to take into account some important biological facts such as the asymmetric lipid composition between the two lipid leaflets composing the plasma membrane. The production of such asymmetric models represents a current challenge and has been hardly investigated yet.

In this context, this master thesis aimed to use the promising microfluidic approach to conceive a device able to produce asymmetric biomimetic liposomes.

To perform the liposome assembly, a microfluidic chip with two successive channel junctions was designed to form the two leaflets of the liposome one after the other. The channels following the second junction were then render hydrophilic with PVA coating. This modification is required to produce liposome and is the most critical step to build a functional microfluidic device.

Two approaches were then considered to produce liposomes with the developed device: the spontaneous transfer across a laminar interface and the droplet emulsion transfer. With the experimental conditions chosen, only the second approach led to the production of liposomes with a size ranging from 92 to 111 µm that still contains some residual octanol. In this approach, W1 droplets formed at the first channel junction, where the inner aqueous phase containing lipids (W1) is sheared by the octanol phase, gave rise to the formation of liposomes at the second channel junction with a maximal success rate of 59%. This success rate is affected when varying the flow rate ratio between the W1 and the octanol phases, which impacts the W1 droplets size. The non-confinement of W1 droplet also impacted negatively the liposome formation. In addition, it was observed that the correct timing for the W1 droplet arrival at the second channel junction is a condition for a successful liposome formation.

Even though the developed device still need to be improved and the liposome asymmetry has not been assessed yet, this work has put strong basis for the conception of a microfluidic device able to generate biomimetic liposomes.

Key words: liposomes, microfluidics, biomimetic model, PVA hydrophilic modification

Résumé

La membrane plasmique est une structure qui joue un rôle clé dans les fonctions cellulaires et de certaines protéines, ainsi que dans la reconnaissance de molécules « allogènes ». Chez les plantes, cette structure, et plus particulièrement sa fraction lipidique, semble impliquée dans la perception d'éliciteurs comme la surfactine, une molécule apportant une potentielle alternative aux pesticides conventionnels.

Toutefois, le développement de ces alternatives nécessite une compréhension de mécanismes biologiques à l'échelle moléculaire. Au vu de la complexité et de la diversité moléculaire de la membrane plasmique de plantes, des modèles biomimétiques simplifiés tels que les liposomes ont été mis au point pour élucider les mécanismes moléculaires en jeu.

Néanmoins, pour être corrélés aux phénomènes biologiques, ces modèles biomimétiques simplifiés doivent tenir compte de caractéristiques biologiques importantes, dont l'asymétrie de composition lipidique entre les deux feuillets de la membrane plasmique. La mise au point de ces modèles asymétriques est un défi actuel qui n'a été que peu étudié.

Dans ce contexte, ce mémoire a pour objectif d'utiliser l'approche prometteuse de la microfluidique pour concevoir un outil capable de former des liposomes biomimétiques asymétriques.

Pour produire ces liposomes, une puce microfluidique avec deux jonctions de canaux successives a été conçue pour assembler les deux feuillets des liposomes l'un après l'autre. Les canaux qui suivent la seconde jonction ont ensuite été rendus hydrophiles à l'aide d'un recouvrement au PVA. Cette modification est nécessaire pour pouvoir former des liposomes et constitue l'étape critique de la fabrication de la puce microfluidique.

Enfin, deux approches ont été considérées pour produire des liposomes avec l'outil développé : le transfert spontané à travers une interface laminaire et le transfert de goutte d'émulsion. Avec les conditions expérimentales utilisées, seule la seconde approche a abouti à la formation de liposomes d'une taille allant de 92 à 111 µm qui contenaient toutefois de l'octanol résiduel. Dans cette approche, les gouttes W1 formées à la première jonction de canaux, où la phase aqueuse interne (W1) est cisaillée par la phase octanol, donnent lieu à la formation de liposomes à la seconde jonction de canaux avec un taux de succès maximal de 59 %. Ce taux de succès est affecté par la variation du ratio de débit entre les phases W1 et octanol, qui modifie la taille des gouttes W1. Le non-confinement de ces gouttes W1 a aussi impacté négativement la formation de liposomes. En outre, il a été observé que le timing correct d'arrivée des gouttes W1 à la seconde jonction de canaux est une condition pour réussir à former des liposomes.

Bien que la puce microfluidique développée nécessite encore d'être améliorée et que l'asymétrie des liposomes n'ait pas encore été évaluée, ce mémoire pose les bases pour la conception d'un outil microfluidique pour produire des liposomes biomimétiques.

Table of content

List of abbreviations

AFM	Atomic force microscopy
ASGs	Acylated steryl glycosides
BAR	Bin-Amphiphysin-Rvs
BODIPY	boron dipyrromethen
CER	Ceramides
CF	5(6)-carboxyfluorescein
Chol	Cholesterol
CL	Cardiolipin
CMC	Critical micellar concentration
DGDG	Digalactosyldiacylglycerol
DIMs	Detergent insoluble membranes
DMPC	1,2-dimyristoyl-sn-glycero-3-phosphocholine
DOPC	1,2-dioleoyl-sn-glycero-3-phosphocholine
DPPC	1,2-dipalmitoyl-sn-glycero-3-phosphocholine
DPPG	1,2-dipalmitoyl-sn-glycero-3- phosphoglycerol
DRMs	Detergent resistant membranes
DSPC	1,2-distearoyl-sn-glycero-3-phosphocholine
ELISA	Enzyme-linked immunosorbent assay
ESCRT	Endosomal Sorting Complex Required for Transport
FTIR spectroscopy	Fourier transform infrared spectroscopy
GIPC	Glycosyl inositol phosphorylceramides
GluCer	Glucosylceramide
GUVs	Giant unilamellar vesicles
ITC	Isothermal titration calorimetry
LB	Langmuir-Blodgett
LCBs	Long Chain Bases
Ld	Liquid-disordered

Lo	Liquid-ordered
LUVs	Large unilamellar vesicles
LS	Langmuir-Schaeffer
MAMPs	Microbial associated molecular patterns
MLVs	Multilamellar lipid vesicles
NMR	Nuclear magnetic resonance
NR	Neutron reflectivity
PA	Phosphatidic acid
PC	Phosphatidylchlonine
PCR	polymerase chain reaction
PDMS	polydimethyl siloxane
PE	phosphatidylethanolamine
PIPs	phosphatidylinositol-phosphates
PLPC	palmitoyl linoleoyl phosphatidyl choline
PM	Plasma membrane
POPC	1-palmitoyl-2-oleoyl-sn- glycero-3-phosphocholine
POPG	1-palmitoyl-2-oleoyl-sn-glycero-3-phosphatidylglycerol
PS	phosphatidylserine
PVA	Polyvinyl alcohol
SANS	Small angle neutron scattering
SAXS	Small angle X-ray scattering
SRF	surfactin
SGs	Steryl glycosides
SLB	Supported lipid bilayer
SM	Sphingomyelin
SPR	Surface plasmon resonance
SUVs	Small unilamellar vesicles
ULVs	Unilamellar lipid vesicles
W1	Inner aqueous phase

W2	Outer aqueous phase
w/o emulsion	Water-in-oil emulsion
w/o/w double emulsion	Water-in-oil-in-water double emulsion

List of figures

List of tables

1. Context

The plasma membrane is a key structure for cell integrity and physiology. This barrier between the inner space of the cell and its external environment is the site of many exchanges and reactions that play an important role in the function of the cell and some proteins. It is also involved into the recognition of some “allogenic” molecules.

In plants, the plasma membrane, and more particularly its lipid fraction, has been suggested to be involved in the perception of elicitors such as surfactin. These molecules stimulate the plant defense response against several biological aggressors, so they represent a potential alternative to conventional pesticides. Nevertheless, the development of such new plant protection products requires to understand the molecular mechanisms at stake.

As the plasma membrane, and particularly the plant plasma membrane, is a very complex structure, the use of simplified models is required to decipher the mechanisms at the molecular level. Biomimetic models such as liposomes have provided useful insights into some biological phenomena. However, these models, though simple, have to take into account some important biological characteristics to be correlated with the biological events. One of these characteristics is the asymmetry of lipid composition between the inner and the outer leaflet of the lipid bilayer composing the plasma membrane.

The production of such asymmetric models is very complex and has been hardly studied yet. A promising approach uses the droplet microfluidic technology.

In this context, this master thesis aimed to develop a microfluidic chip to produce asymmetric liposome in a reproducible manner and with a minimum of steps.

2. Introduction

2.1. Importance of lipids in plant plasma membranes

Lipids are one of the major components of the plasma membrane (PM). As represented in figure 1, this barrier that separates the inner space of the cell, the cytoplasm, from the external environment is composed of a lipid bilayer where several proteins can be embedded or anchored to the PM (Taiz et al., 2015). In terms of mass content, lipid-to-protein ratio in tobacco PM was experimentally estimated at around 1.3 (Cacas et al., 2016), corresponding to a molar ratio of 1 protein for 50-100 lipid molecules (Furt et al., 2011; Mamode Cassim et al., 2019). As the PM delineates the interface between the cell and the environment, it is a key structure for signal recognition and transduction into intracellular responses for nutritional uptake/distribution, environmental responses, and developmental signaling (Furt et al., 2011; Mamode Cassim et al., 2019).

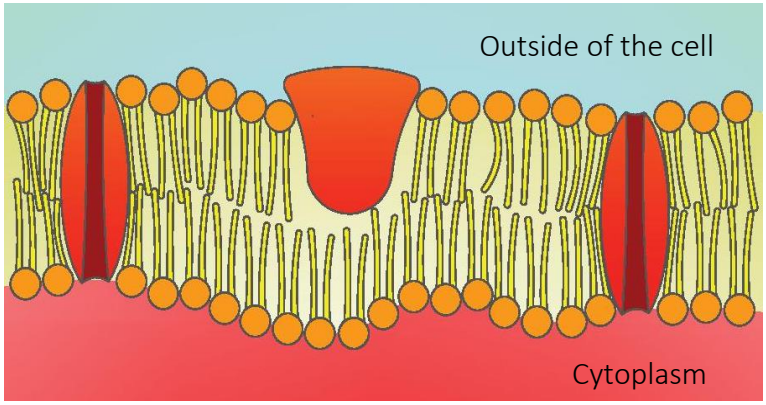

Figure 1 Schematic representation of the structure of a plasma membrane

Even though the organization of PM lipids seems very simple, with a lipid bilayer where the polar headgroups are facing the aqueous environment and the hydrocarbon tails facing the interior of the bilayer, this bilayer is actually highly organized, laterally and transversally, with a wide structural range of lipids. As a matter of fact, cells use about 5% of their genes to produce all their lipids, mainly synthetized in the endoplasmic reticulum and the Golgi apparatus (van Meer et al., 2008). Furthermore, proteins such as Bin-Amphiphysin-Rvs (BAR) domain proteins, tetraspanins, ESCRT, septins, actin or flippase regulate the organization of lipid PM (Rossy et al., 2014). Except for septins that are only found in green algae, all of these families of proteins are present in plants (Yamazaki et al., 2013; Zhuang et al., 2013; Sheetz et al., 2014; Spitzer et al., 2015; Jimenez-Jimenez et al., 2019; Nintemann et al., 2019; Palmgren et al., 2019).

According to the fundamental biological maxim that "structure subserves function", all these observations suggest that this complex lipid organization is important for biological functions. In the past decades, several studies and reviews investigated the biological importance of PM lipids highlighting their potential role in PM function and signal transduction (van Meer et al., 2008; Mongrand et al., 2010; Mamode Cassim et al., 2019).

The PM lipid bilayer is a carefully balanced environment. Still, several amphiphilic molecules are able to interact with it, inflicting changes in its structure balance that can lead to antibiotic activities or stimulation of plant defense response (Seddon et al., 2009; Henry et al., 2011; Zhao et al., 2019). These changes must be considered with the overall effect that they may have on the function and integrity of the membrane. The development of tools/strategies to better understand the mechanisms at the molecular level is therefore of crucial importance.

2.1.1. Lipid composition and organization of the plant plasma membrane

Three main classes of lipids compose the PM: glycerophospholipids, sphingolipids and sterols (Deleu et al., 2014; Cacas et al., 2016). Still, as shown in Table 1, the proportion and the composition of each class can vary among species (Deleu et al., 2014).

Table 1 Proportion, in molar %, of the three main lipid classes of different cell membranes in eukaryotic and prokaryotic cells. The most abundant lipids of these classes are indicated in bracket. (Tjellström et al., 2010; Deleu et al., 2014; Cacas et al., 2016)

Lipid class	Eukaryotic cell					prokaryotic cell	
	human erythrocyte	*S. cerevisiae*	*A. thaliana* leaves	*Avena sativa* var. belinda root	*N. tabacum* leaves	*S.aureus* Gram +	*E. Coli* Gram -
Glycerolipids	39.5 (PC and PE)	54 (PC and PE)	47 (PE and PC)	33	30 (PE and PC)	100 (PS and CL)	100 (PE and CL)
Sphingolipids	14 (SM)	10-20	7 (GIPC)	20	45 (GIPC)		
sterols	46 (Chol)	30-40	46 (sitosterol)	47 (stigmasterol)	25		
other	0.5						
reference	(Deleu et al., 2014)	(Deleu et al., 2014)	(Deleu et al., 2014)	(Tjellström et al., 2010)	(Cacas et al., 2016)	(Deleu et al., 2014)	(Deleu et al., 2014)

PC : phosphatidylcholine, PE : phosphatidylethanolamine, PS : phosphatidylserine, CL : cardiolipin, SM : sphingomyelin, GIPC : glycosyl inositol phosphoryl ceramides, Chol : cholesterol

Paying more attention to the plant PM, the two major phospholipids are phosphatidylcholine (PC) and phosphatidylethanolamine (PE) with palmitic and linoleic acids as main acyl chains and phosphatidylglycerol (PG), phosphatidylinositol (PI), phosphatidic acid (PA) and phosphatidylserine (PS) are minor phospholipids (Furt et al., 2011; Mamode Cassim et al., 2019). Although they account for a minor fraction of total phospholipids, polyphosphoinositides and phosphatidylinositol-phosphates (PIPs) are important lipids involved in many regulatory processes, such as cell signaling and intracellular trafficking (Xue et al., 2009; Mamode Cassim et al., 2019).

In addition to phospholipids, the plant PM is always enriched in sterols and sphingolipids (Deleu et al., 2014).

Sterol are isoprenoids characterized by a cylcopentaperhydrophenantren moiety, made up of four rigid rings and hydroxylated at position 3. In contrast with animals and yeast membranes that incorporate only one sterol (cholesterol and ergosterol, respectively), plant membranes contain multiple sterol species (Furt et al., 2011). As an example, 61 sterols and pentacyclic triterpenes have been identified in maize seedlings (Guo et al., 1995). The main difference between mammalian cholesterol (Chol) and phytosterols is an extra alkyl group in the C24 position in the side chains (figure 2A). Sitosterol is the most abundant plant sterol in most species reported including the plant model Arabidopsis, except for a few cases such as stigmasterol in tobacco, spinasterol in Medicago and isofucosterol (Δ-5 avenasterol) in many plants (Mamode Cassim et al., 2019). In addition, phytosterols can be derived into phytostanols, steryl glycosides (SGs) and acylated steryl glycosides (ASGs) (figure 2 B and C). Phytostanols are the saturated analogues of sterols with no double bond in the rings. SGs are sterols acylated with sugar moiety attached to the 3- hydroxy group at the C3-atom of a sterol and a hydrocarbon side chain at C17 (figure 2C left). The number of sugars and the configuration of their linkage to the sterol may vary, the most common sugar moiety being the pyranose form of D-glucose (Mamode Cassim et al., 2019). SGs may be further acylated into ASGs (figure 2C right), increasing the diversity of phytosterols. Usually, this acylation occurs at the C6-atom of the sugar moiety with palmitic, oleic and less frequently with stearic, linoleic, and linolenic acid (Mamode Cassim et al., 2019).

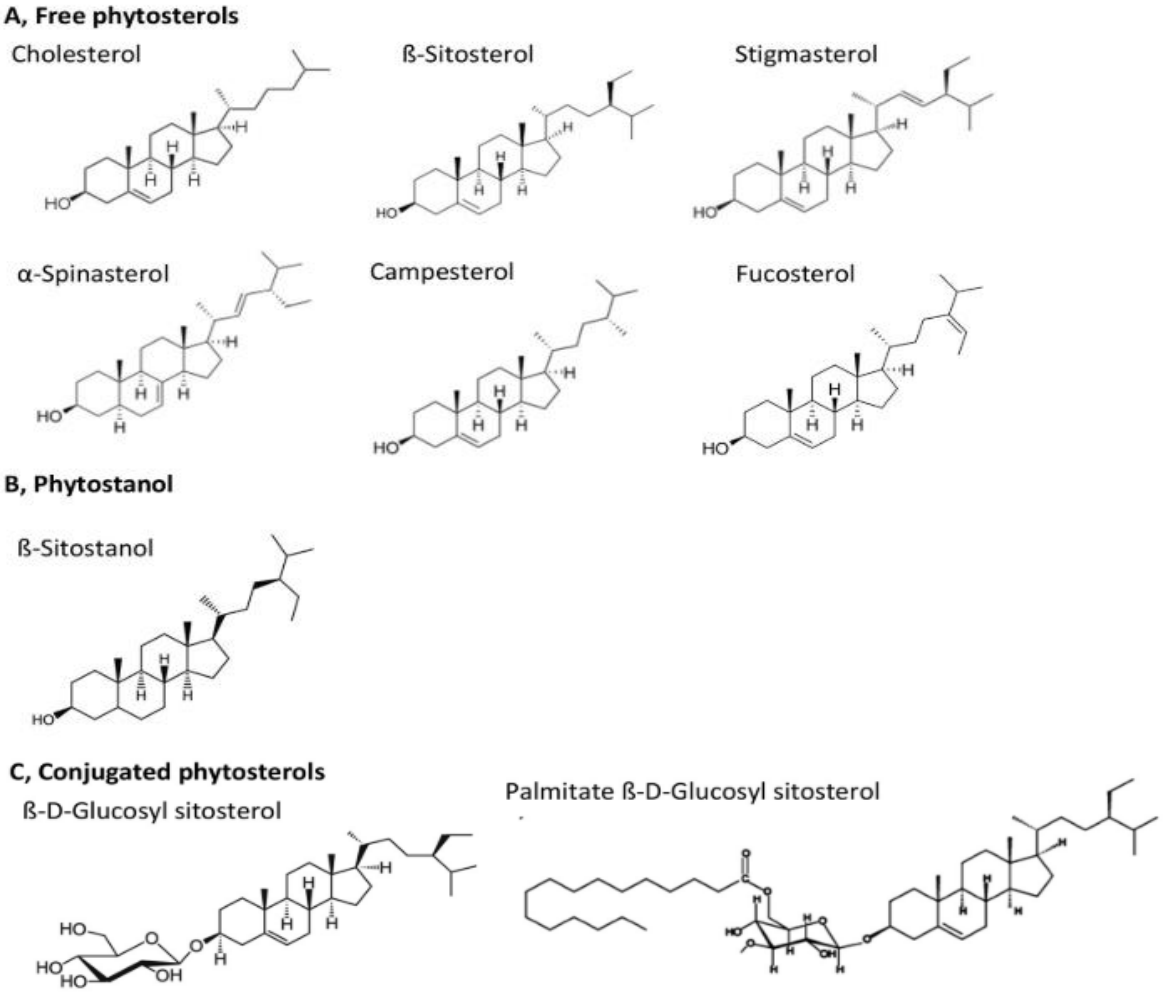

Figure 2 Structures of specific plasma membrane phytosterols compared with animal cholesterol. A, free phytosterols; B, phytostanol; C, conjugated phytosterols (adapted fom Mamode Cassim et al., (2019))

Sphingolipids are divided in four groups: ceramides (Cer), glucosylceramide or cerebroside (gluCer), Glycosyl Inositol Phosphoryl Ceramides (GIPC) and free Long Chain Bases (LCBs) accounting for 2, 34, 64 and 0.5 % respectively in *Arabidopsis thaliana* (Mamode Cassim et al., 2019). Their structure and synthesis have been recently reviewed by Michaelson et al. (2016). Briefly, the chemical structure of sphingolipids consists in a long chain base (LCB) that can be amidated with a fatty acid to form ceramides. In plants, up to eight different molecular moieties can be formed from the most basic LCB, sphinganine, that has an acyl chain of 18 carbon atoms with two alcohol residues at C1 and C3 and an amine residue at C2 (Furt et al., 2011). Ceramides can be further modified into inositol phosphoryl ceramide (IPC) via the head group transfer of phosphatidylinositol onto a Cer catalyzed by IPC synthase. Then, the addition of simple or

multiple sugars on Cer at the C1 position or on the inositol group of IPC can produce GluCer or GIPC respectively (figure 3) (Michaelson et al., 2016).

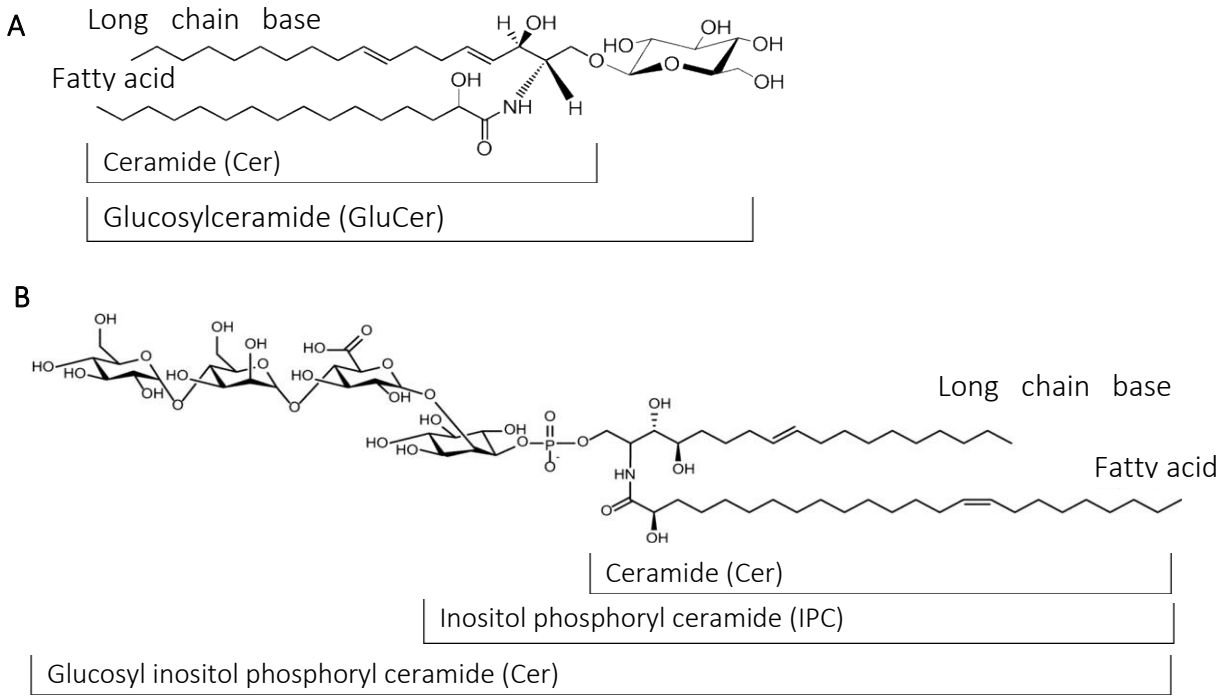

Figure 3 Example of structure of (A) glucosylceramide (GluCer) and (B) glucosyl inositol phosphoryl ceramide (GIPC) (Cacas et al., 2012; Fang et al., 2016)

Along with this diversity of lipids, plant PM shows a heterogeneous lateral distribution in each leaflet with the presence of different phases, micro- and nano-domains and also a transversal lipid asymmetry between the outer and the inner leaflet. This organization can be due to intrinsic factors such as lipid-lipid or lipid-protein interactions and extrinsic factor, for example, interconnection with cell component or the cell wall (Gronnier et al., 2018).

The lateral segregation of lipids is supposed to be driven by the interaction between sphingolipids and sterols, the latter having self-association properties with the highly saturated hydrocarbon chains of sphingolipids (Mongrand et al., 2010). These properties lead to the formation of a liquid-ordered (Lo) phase enriched in sterols and sphingolipids, called lipid rafts, separated from the liquid-disordered (Ld) phase of the PM (Mongrand et al., 2010; Nyholm, 2015; Cacas et al., 2016). Besides, several proteins play a role in the PM lipids sorting and segregation, thereby affecting membrane curvature (Cacas et al., 2012; Rossy et al., 2014). These Lo domains have been shown to be more resistant to solubilization by detergents than the Ld ones and the study of rafts is therefore often linked with the study of detergent resistant membranes (DRMs), also called detergent insoluble membrane (DIMs) (Lichtenberg et al., 2005; Cacas et al., 2012).

These lipid rafts impose spatial and temporal regulation on interfacial protein binding and/or enzymatic reaction (Furt et al., 2011). The lipid environment may also affect the conformation of transmembrane protein domains and/or the activation and recruitment of specific proteins involved in physiological function such as vesicle formation and signal transduction (Cacas et al., 2012; Fezoua-Boubegtiten et al., 2019). Proteomic studies of plant DIMs reveal a high number of signaling proteins (Cacas et al., 2012). Lipid rafts are indeed supposed to be involved, at the micrometer scale, in processes of growth and development and also, at the nanometer scale, in dynamic processes regulating signal transduction in response to environmental stress (Mongrand et al., 2010).

Next to the lateral organization of lipids, their asymmetric distribution between both PM leaflets is also well documented in animal field. This asymmetric distribution has implications into vesicle transport, protein recruitment and function, signal transduction, and physiological issues like cell death and blood clotting (van Meer, 2011). Only a few publications addressed experimentally the asymmetry of the plant plasma membrane. In root plasma membrane of oat, it was shown that digalactosyldiacylglycerol (DGDG) was exclusively located in the inner leaflet together with 60% of phospholipids(Tjellström et al., 2010). In tobacco, as illustrated in figure 4, GIPC are mostly located on the outer leaflet of the PM (Cacas et al., 2016). Based on these results, Mamode Cassim et al (2019) recently proposed a model for the distribution of lipids in the plant PM where : 1/GIPC and GluCer are exclusively located in the outer-leaflet; 2/sterols (free and

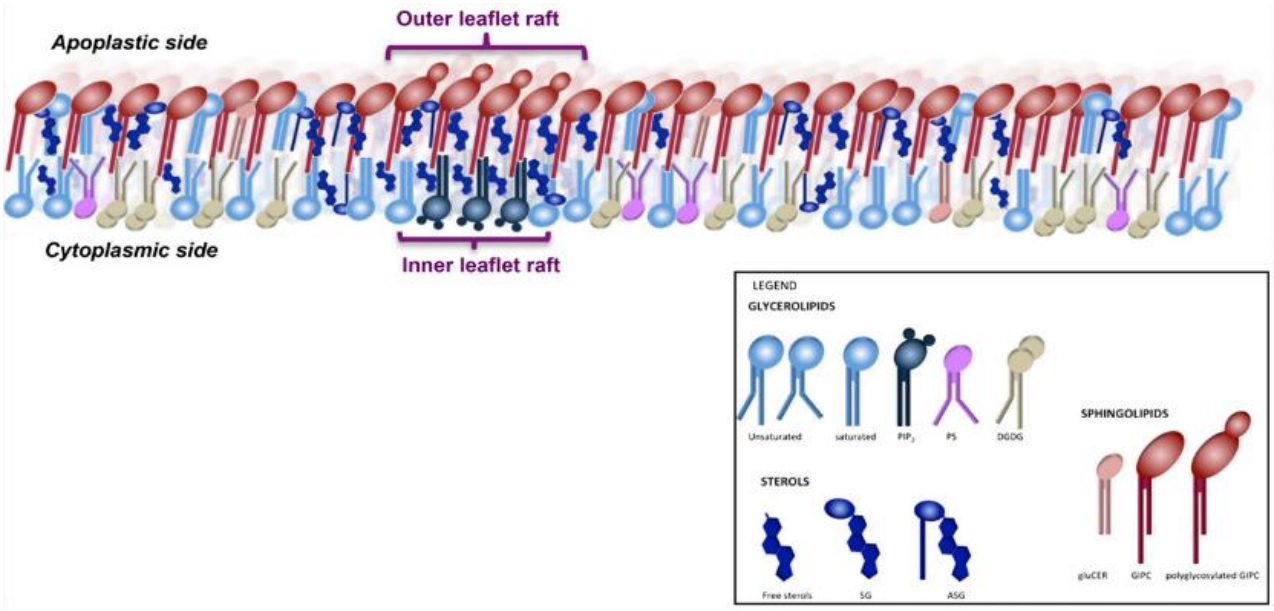

Figure 4 Model for the organization of lipids in tobacco PM built by Cacas et al., (2016). They hypothesize that GIPCs are located exclusively in the apoplastic face. DGDG, Digalactosyldiacylglycerol; PS, phosphatidylserine (adapted from Cacas et al., (2016))

conjugated) are enriched in the outer leaflet; 3/phospholipids are enriched in the inner-leaflet with PIPs, 4/PS, PA exclusively in the inner leaflet.

The asymmetry of lipid membranes may influence the protein association with Lo phase (Nyholm, 2015). Hussain et al. (2013) conducted experiments comparing the affinity of human integrin proteins with the lipid bilayer. They demonstrated that these proteins have a higher affinity with the Lo phase over the Ld phase when incorporated into asymmetric bilayers, containing Lo phase only in the outer leaflet, while the opposite is observed with symmetric bilayers. This observed phenomenon might be partially explained by the difference of hydrophobic thickness between the Lo domains and the Ld domains but lipid-protein interactions play also a role (Hussain et al., 2013). The importance of lipid-protein interaction was also highlighted by Kamiya et al. (2016) and Lin et al. (2014a). Indeed, the reconstitution rate of the membrane protein Cx43 in asymmetric giant unilamellar vesicles (GUVs) was influenced by their composition, which impacts the charges of the membrane (Kamiya et al., 2016). Moreover, an experiment with asymmetric LUVs and Perfringolysin O showed that the stable formation of the membrane-inserted intermediate seems to depend on the inner leaflet lipids, whereas the high midpoint for initial interaction with Chol and for insertion is mainly determined by the outer leaflet lipids (Lin et al., 2014a).

In addition, the organization of both leaflets is influenced by their respective composition and organization through the leaflet coupling. An experiment conducted on asymmetric bilayers suggests that if the outer leaflet of the plasma membrane contained small, ordered SM-enriched domains, the inner leaflet would be locally affected, just in spatial correspondence to the SM domains, via interleaflet coupling (Chiantia et al., 2012). This coupling has significant implications for biological functions as it provides membranes with a platform for co-localization of signaling components, allowing cells to tailor their responses by spatially organizing the molecules involved in G-protein-coupled receptors signal transduction (Nickels et al., 2015). In addition, physical properties of the bilayer such as its bending rigidity, related to how much energy is needed to deform it, are also impacted by the asymmetric distribution of lipids. In fact, when varying distribution of lipids between both leaflets in a simple model considering the curvature elastic energy of the two monolayers separately and assuming a constant bilayer composition, the minimum curvature energy of the bilayer is reached when the bilayer is symmetric (Elani et al., 2015). This prediction was consistent with the experiment comparing the bending rigidity of symmetric GUVs of POPC (1-palmitoyl-2-oleoyl-sn- glycero-3-phosphocholine) or DOPC (1,2-dioleoyl-sn-glycero-3-phosphocholine) and asymmetric GUVs with an inner leaflet of POPC and an outer leaflet of DOPC (Elani et al., 2015; Karamdad et al., 2016).

The indication that asymmetry has a stark effect on mechanical properties of the membrane has immediate consequences for the study of membrane proteins which may be regulated by membrane mechanics (Elani et al., 2015). Plants have indeed three families of mechanosensitive channels named MscS-Like (MSL) channels, two-pore domain K+ (TPK) channels and Mid1-complementing activity (MCA) channel which are involved in stress response, osmoregulation or plant development (Basu et al., 2017). The asymmetry may also bring mechanical changes across the membrane affecting the mechanisms of cell endo- and exocytosis (Karamdad et al., 2016).

2.2. Biomimetic membranes

The existence of lipid heterogeneity with a lateral segregation in domains, different phases and an asymmetric distribution of lipids between leaflets along with the importance of lipids chemical diversity makes PM a very intricate structure. This complexity is further increased considering that PM is an association of lipids, proteins and carbohydrates that can interact, rendering the study of cell biology a difficult task. To alleviate this, simplified artificial membrane systems mimicking the lipid composition of biological membranes have been developed (Deleu et al., 2014; Salehi-Reyhani et al., 2017).

Among the developed systems, three are commonly used and illustrated in figure 5: the lipid monolayer, the supported lipid bilayer and the liposome or lipid vesicle (Deleu et al., 2014).
Each of these systems can provide different and complementary information using their associated technique as presented in table 2 (Heerklotz et al., 2004; Buchoux et al., 2008; Zhao et al., 2012; Deleu et al., 2014; Nickels et al., 2015; Buscema et al., 2019; Nielsen et al., 2019).

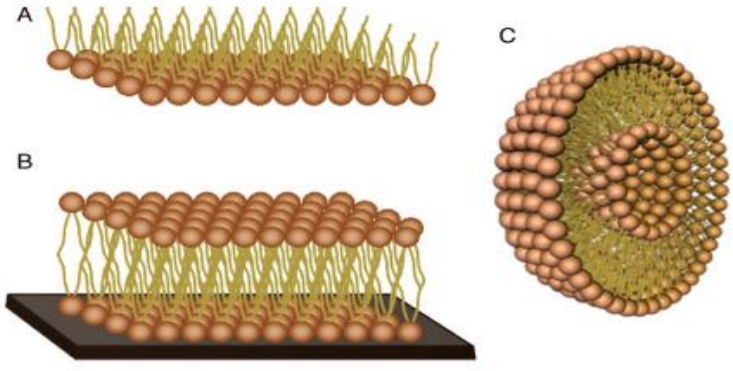

Figure 5 Schematic representation of membrane model: (A) lipid monolayer, (B) supported lipid bilayer, (C) liposome (adapted from Deleu et al., 2014)

Table 2 Examples of techniques associated with a membrane model and information provided by these ones (Heerklotz et al., 2004; Buchoux et al., 2008; Zhao et al., 2012; Deleu et al., 2014; Nickels et al., 2015; Buscema et al., 2019; Nielsen et al., 2019)

Membrane model	Associated technique	Studied property
Lipid monolayer	Langmuir trough	- Monolayer formation, molecular area, monolayer phases, monolayer stability, two-dimensional compressibility and interaction of species from the subphase with the monolayer - Penetration ability of a molecule - Attractive effect of the lipids, lipid specificity
	Surface plasmon resonance (SPR)	- Real-time affinity, selectivity and kinetics of biomolecular interactions
	IRRAS or PM-IRRAS	- Chemical moieties involved in the interaction between molecules of interest and the membrane
Supported lipid bilayer	Atomic Force Microscopy (AFM)	- Observation of phase separated domains - Study the lipid selectivity of interacting molecule - Observation of the interacting molecule effect on lateral structure/organization of the lipid bilayer
	Neutron reflectivity (NR)	- Transversal bilayer structure and thickness with a precision down to an angstrom scale
	Surface plasmon resonance (SPR)	- Real-time affinity, selectivity and kinetics of biomolecular interactions
	Electron paramagnetic resonance (EPR)	- Ordering, mobility and polarity of phospholipids and mobility of exogenous agent within the membrane
Liposome	Isothermal titration calorimetry (ITC)	-Thermodynamic characterization of molecule interactions with model lipid membrane - Membrane lysis and solubilization
	Fluorescence spectroscopy	- Molecule impact on membrane integrity, destabilization and packing
	FTIR-ATR	- Chemical moieties involved in the interaction between molecules of interest and the membrane
	Small angle neutron scattering (SANS)	- Lateral structures of lipid membranes of structure from ۱ to ۱۰۰ nm and transversal bilayer structure and thickness
	small angle X-ray scattering (SAXS)	- transversal bilayer structure and thickness
	Solid-state NMR spectroscopy	- Membrane order and dynamics

2.2.1. Lipid monolayers

Lipid monolayers (figure 5A) are formed at the water-air interface of a Langmuir trough by spreading lipids of the considered membrane on the water surface (Deleu et al., 2014; Sebaaly et al., 2019). This technique provides a simple model considered as half the lipid bilayer of biological membranes. This model is useful to characterize the interaction of a molecule of interest with lipids and its ability to penetrate the outer

leaflet (Eeman et al., 2010; Sebaaly et al., 2019). Even though lipid monolayers are constituted of only one lipid leaflet and therefore do not reflect the complexity of biological membrane structure, this model displays the ability to vary parameters such as the nature and the packing of the spread lipids, the composition of the subphase (pH, ionic strength) and the temperature in a controlled way and without limitation (Eeman et al., 2010).

2.2.2. Supported lipid bilayers

The second model, namely the supported lipid bilayer (SLB) (figure 5B), is composed of a lipid bilayer supported onto a solid surface such as mica, glass or quartz wafers. SLBs can be formed by the Langmuir-Blodgett (LB) technique, by a combination of the LB and Langmuir-Schaeffer (LS) techniques, by fusion of lipid vesicles onto the solid supports or by surfactant depletion from micellar solutions composed of a mixture of surfactants and phospholipids (Jonathan M. Crane et al., 2005; Peetla et al., 2009; Eeman et al., 2010; Nickels et al., 2015). When prepared with a sequential deposition of lipid monolayer using LB technique, a combination of LB and LS or a combination of LB and vesicle fusion, asymmetric SLBs can be obtained (Deleu et al., 2014; Nickels et al., 2015).

One of the main drawbacks of classical SLB is the proximity between the lipid bilayer and the solid substrate, which may affect the membrane properties of the biomimetic system. Moreover, regarding the asymmetry, care must be taken as the asymmetric bilayers prepared by this way may not have the intended lipid compositions in the two leaflets, due to the flip-flop properties of lipids of the membrane which are known to spontaneously exchange within the two leaflets. In order to maintain the asymmetry over time and to space the bilayer from the solid support, tethered or polymer-cushioned support have been developed (Eeman et al., 2010; Nickels et al., 2015; Sebaaly et al., 2019). SLBs are a useful tool to investigate the lipid domain formation in biological membranes but also to study their interaction with membrane proteins (Deleu et al., 2014; Sebaaly et al., 2019).

2.2.3. Liposomes

Liposomes or lipid vesicles (figure 5C), representing the third model, are spherical vesicles composed of one (unilamellar lipid vesicle, ULVs) or more (multilamellar lipid vesicles, MLVs) lipid bilayers surrounding an aqueous core (Sebaaly et al., 2019). According to their size, ULVs can be divided into three categories. Small unilamellar vesicles (SUVs) usually exhibit a mean diameter ranging from 20 to 100 nm, large

unilamellar vesicles (LUVs) from 100 to 1000 nm and giant unilamellar vesicles (GUVs) have a size over 1 µm (Siontorou et al., 2017; Sebaaly et al., 2019).

As a biomimetic model, unilamellar vesicles have more physiologically relevant hydration, natural boundary conditions, and enable facile incorporation of membrane proteins. Their flexibility in terms of size (or curvature) is also interesting: SUVs are ideal for mimicking highly curved membranes such as endosomes or synaptic vesicles, whereas GUVs are suitable for very low curved membranes like the cell plasma membranes (Nickels et al., 2015). The size of GUVs also allows light microscopic imaging which cannot be achieved with SUVs (Zhao et al., 2012). These models are commonly used to study membrane phase behavior and membrane processes such as membrane fusion, molecular recognition, cell adhesion, and membrane trafficking (Deleu et al., 2014). Liposomes are also reported as artificial cell models in order to study the mechanisms of action of various structural components and associated machineries such as cytoskeleton biophysics (Salehi-Reyhani et al., 2017). In addition to their application as biomimetic membranes, SUVs are widely used for biomedical and biotechnological purposes, for example, as drug carriers or to estimate the efficiency of a drug (Peetla et al., 2009; Carugo et al., 2016; Sebaaly et al., 2019).

Several methods have been developed to produce liposomes. Classical methods produce vesicles with a symmetric lipid composition between leaflets. All of these methods start from the hydration of a dried lipid film with the desired buffer. The dried lipid film is obtained by slow evaporation of a lipid solution in a volatile organic solvent (Pomorski et al., 2014). The film hydration produces then multilamellar vesicles that can form LUVs or SUVs when extruded or sonicated. When extruded, multilamellar vesicle suspensions can be disrupted either by several freeze–thaw cycles or by prefiltering the suspension through a larger pore size prior extrusion to improve the homogeneity of size distribution of the vesicles (Zhao et al., 2012).

GUVs are formed by the gentle hydration method or the electroformation method (Pomorski et al., 2014; Kamiya et al., 2017). The first approach consists in the hydration of a dried lipid film with an aqueous solution inducing the swelling of the phospholipid film and producing GUVS. The second approach is an improvement of the first one where an oscillating electric field across the lipid film is applied during the swelling to accelerate the process.

All the previously mentioned methods only allow the formation of liposome with a symmetric lipid distribution, which represents an important drawbacks as the lipid asymmetry is naturally found in native biological membranes (Eeman et al., 2010).

In order to produce a more realistic model, techniques have been developed for asymmetric vesicles formation. One of them was developed by Cheng et al. (2009) and consists in cyclodextrin-induced lipid exchange to prepare SUVs with stable asymmetric lipid compositions. The principle of this method is to mix and incubate with cyclodextrin two populations of vesicles previously prepared: unilamellar vesicles (ULVs) with the desired inner leaflet composition and MLVs with the desired outer leaflet composition (figure 6). Several types of cyclodextrin can be used in this technique and their choice depends on the desired lipid composition, with methyl-β-cyclodextrin useful for lipid system without Chol and hydroxypropyl- α-cyclodextrin when Chol is present in the acceptor ULVs (Cheng et al., 2009, 2011; Huang et al., 2013; Lin et al., 2014b; Nickels et al., 2015).

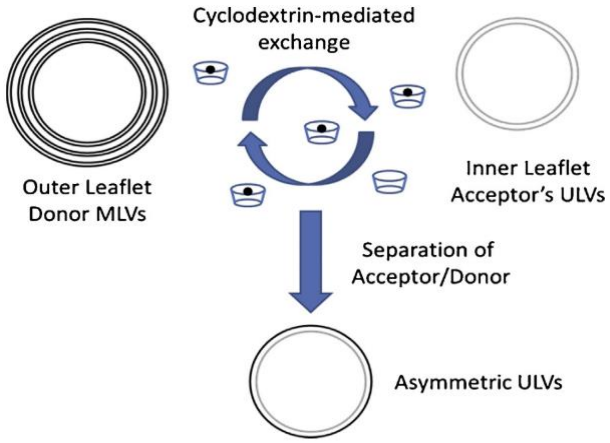

Figure 6 Schematic of asymmetric vesicle production through cyclodextrin mediated exchange developed by Cheng et al. (2009) (adapted from Nickels et al. (2015))

Another possible concept to produce asymmetric vesicles implies protocell systems. With the use of ATP-dependent enzymes called flippases, floppases or scramblases, which are known to maintain the lipid asymmetry in biological membrane, the protocell will be able to generate and maintain membrane asymmetry between the two membrane leaflets in a self-contained manner (Nickels et al., 2015).

Finally, a growing interest is given to microfluidic approaches to synthetize asymmetric liposomes (Matosevic et al., 2013; Lu et al., 2015; Karamdad et al., 2016).

2.3. Microfluidic methods for liposome formation

In recent decades, microfluidic technology has been rapidly developed due to its interesting advantages of system miniaturization and automation. These advantages include the parallelization through multiplexing to achieve high-throughput assays at low cost, the ability to control, monitor and manipulate tiny amounts

of samples at nano- to pico-liter scale and even improvements on analytical performance and sensitivity. The small dimensions of microfluidics devices also imposed a laminar flow regime that give fine control over the temporal and spatial microenvironment.

These interesting properties allowed the development of the droplet microfluidic technology. This technology is based on the production of droplets when two or more immiscible fluid streams are brought into contact with another one (Anna, 2016). To bring the continuous phase (i.e. the fluid out of the droplet) into contact with the dispersed phase (i.e. the fluid inside the droplet) and generate droplets, several junction geometries exist such as T-junction, co-flow and flow focusing (figure 7) (Zhao, 2013).By regulating the size of the channels, the flow rates of the continuous and the dispersed phase and by adjusting the surface tension between fluids with the addition of surfactants, a fine and tunable control on the droplet size can be achieved with very low size dispersity (van Loo et al., 2016; Liu et al., 2017). As droplets are separated from each other with the outer phase, it is possible to generate confined micro-reactors for chemical and biological studies. Droplet microfluidics has indeed been used to perform polymerase chain reaction (PCR), drug screening and toxicity evaluation, cytometry, cell cultivation and bioprocess studies and enzyme-linked immunosorbent assays (ELISA) (Marques et al., 2017; Cui et al., 2018; Kim et al., 2018; Scheler et al., 2019; Shi et al., 2019).

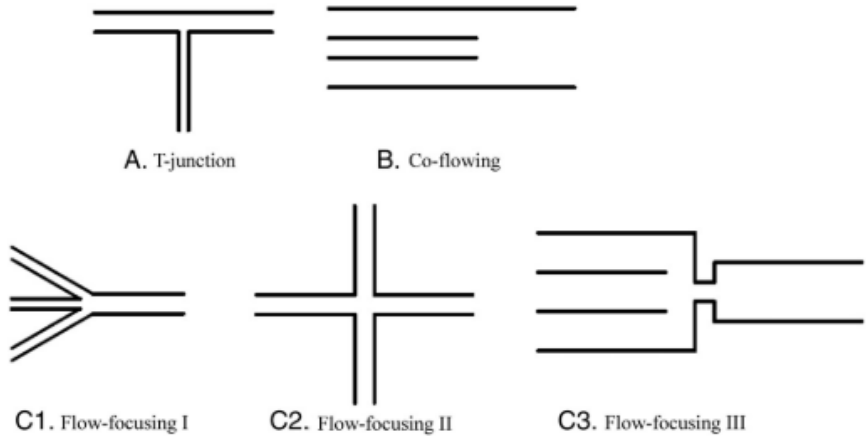

Figure 7 Three types of microfluidic devices. A) T-junction; B) co-flowing; C) flow-focusing, including flow-focusing I, II and III (reproduced from Zhao (2013))

Using droplet microfluidics, several approaches have been developed to produce GUVs with a high control on their size, size distribution and lamellarity by changing the velocity of the solution flow within microdevices or the shapes of the microdevices. Kamiya and Takeuchi (2017) have recently reviewed some of the methodologies developed to produce liposomes with microfluidics. Three main techniques are explored: the droplet emulsion transfer (Matosevic et al., 2011; Karamdad et al., 2015; Lu et al., 2015), the

water-in-oil-in-water (w/o/w) double emulsion (Deng, Yelleswarapu, et al., 2016; Deshpande et al., 2016, 2018) and the pulse jet flow (Kei Funakoshi et al., 2007; Kamiya et al., 2016) (figure 8).

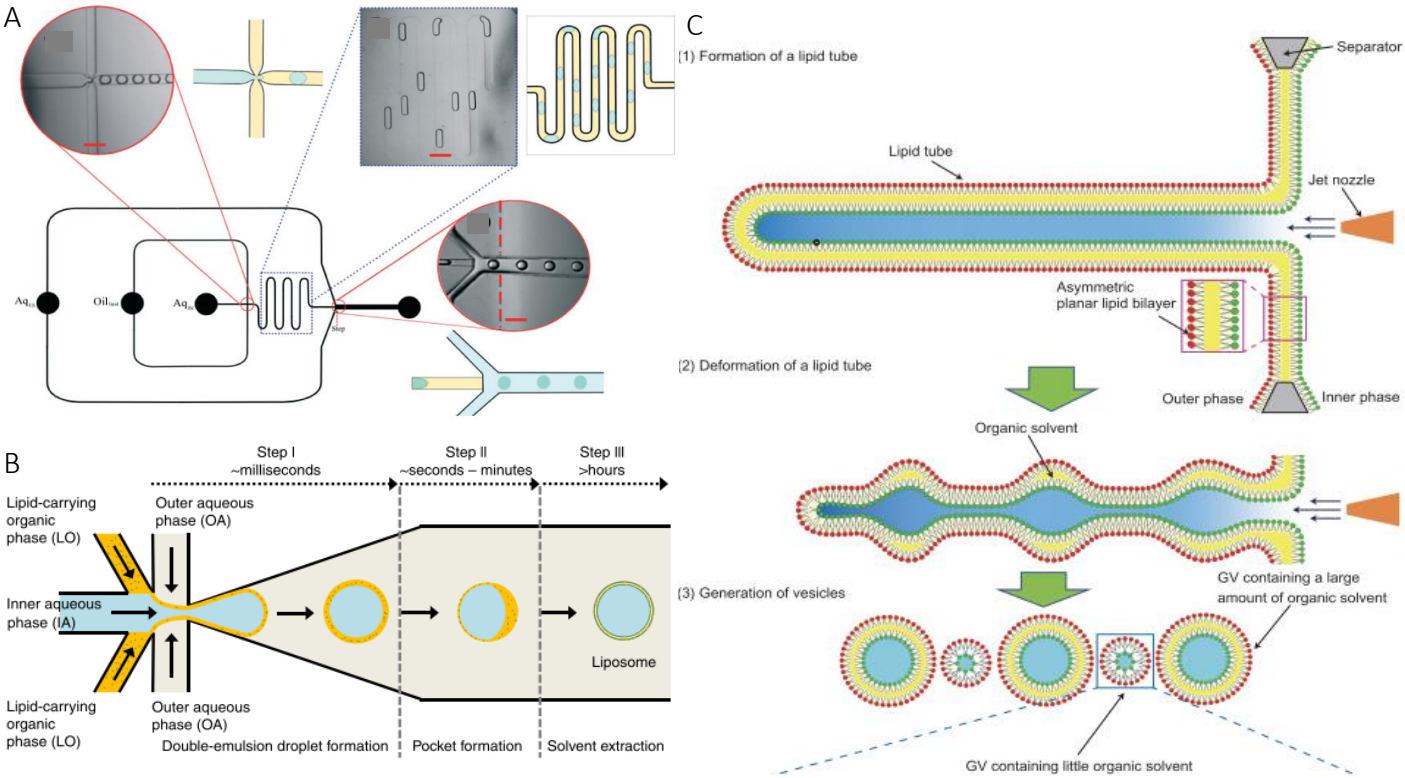

Figure 8 Microfluidic methods to produce liposomes. (A) Droplet emulsion transfer (reproduced from Karamdad et al., 2015). (B) Water-in-oil-in-water double emulsion (reproduced from Deshpande et al., 2016). (C) Pulse jet flow (reproduced from Kamiya et al., 2016)

2.3.1. Droplet emulsion transfer

The droplet emulsion transfer method was first reported by Pautot et al. (2003). Firstly, a simple water-in-oil (w/o) emulsion is prepared by dispersing an aqueous solution into a phospholipid solution dissolved in an organic solvent such as squalene, oleic acid or mineral oil. Then, the w/o emulsion is transferred to an aqueous solution and when the emulsionned droplets cross the second oil-water interface, giant liposomes are formed. Using this approach, several microfluidics devices were developed (figure 9).

Matosevic and Paegel (2011) reported a microfluidic assembly line (figure 9A) to produce symmetric liposomes with size ranging from 20 to 70 µm. This device begins with flow-focusing generation of lipid-stabilized w/o emulsion. The generated droplets are then transferred into the external aqueous phase thanks to a triangular guide in the microchannel, and giant liposomes are then generated through layer-by-layer assembly. However, the proposed device assembles vesicles with an efficiency of only 5% of w/o droplets generated for midsized vesicles. This efficiency drops off to less than 1% as the droplet size falls

outside this range. Larger droplets prematurely contact the interface and merge with the external aqueous flow and smaller droplets are more easily lost in the oil-skim channel.

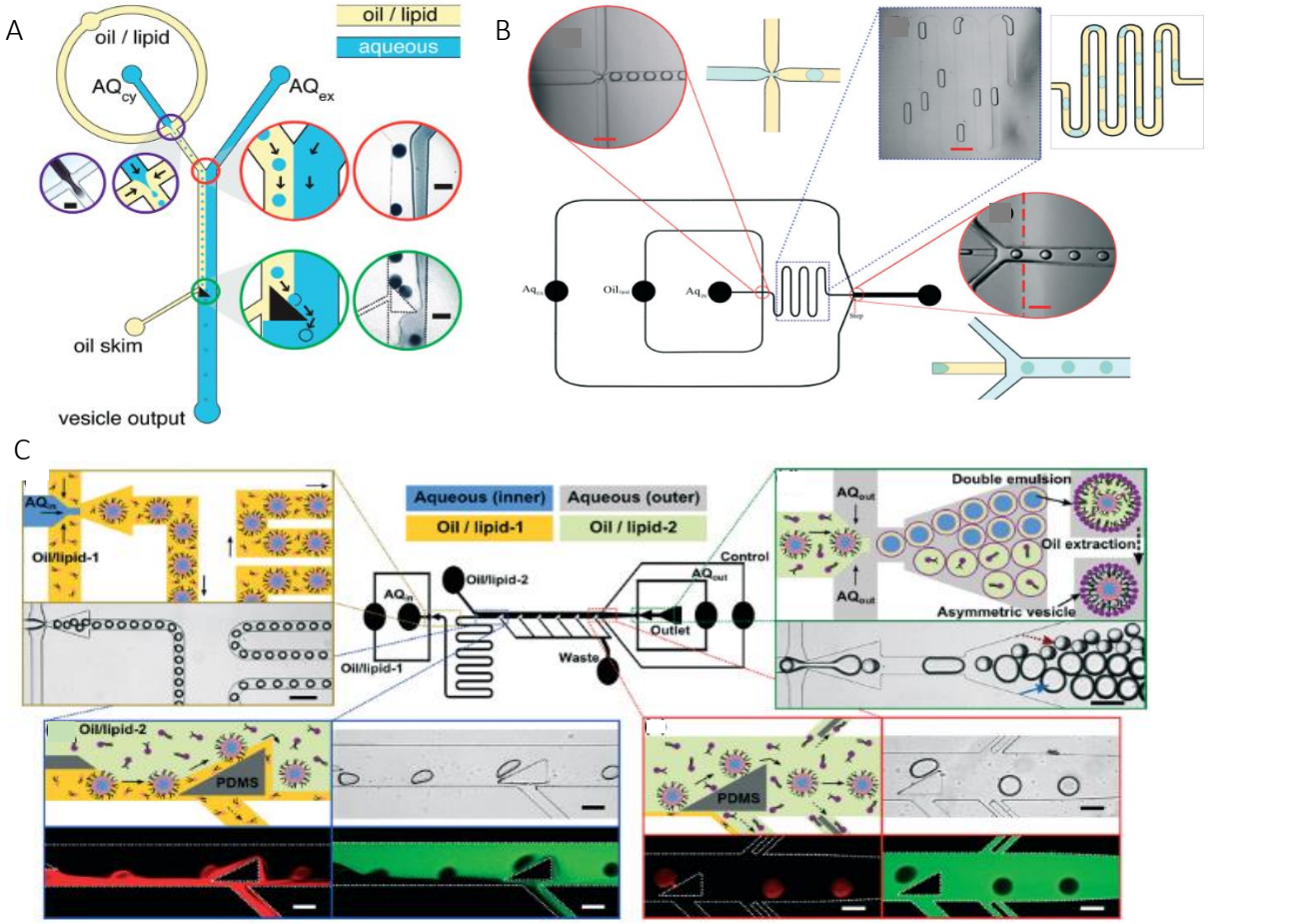

Figure 9 (A) Representation of the liposome assembly line developed by Matosevic and Paegel. Reprinted from Matosevic and Paegel (2011). (B) Schematic and images of the giant liposome formation device developed by Karamdad et al. Reprinted from Karamdad et al. (2015). (C) Schematic and images of the giant liposome formation device developed by Lu et al. Reprinted from Lu et al. (2015)

The transfer of w/o emulsion droplets across a laminar interface to produce liposomes was also suggested by Deng, Wang, et al. (2016). They demonstrate that this transfer is spontaneous if the spreading coefficient (S_i) of the three phase system, defined as $S_i = \gamma_{jk} - (\gamma_{ij} + \gamma_{ik})$ where γ_{ij} is the surface tension between the fluid I and j, is favorable. This spreading coefficient reflects the interfacial energies present in the system. As

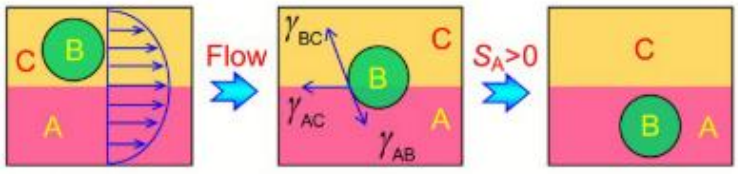

Figure 10 Schematic illustration of the wetting induced transfer of droplets across a laminar liquid-liquid interface in microchannels (reprinted from Deng, Wang, et al. (2016))

shown in figure 10, if $S_A > 0$, i.e $\gamma_{BC} - (\gamma_{AB} + \gamma_{AC}) > 0$, the drop B will transfer from phase C to phase A to reduce the interfacial energies of the system (Deng, Wang, et al., 2016; Deng, Yelleswarapu, et al., 2016).

Karamdad et al. (2015) has built another device where w/o droplets are formed with a flow-focusing junction in a lipid-containing oil flow. The droplets are then transferred across an oil–water interface, facilitating the self-assembly of a phospholipid bilayer (figure 9B). GUVs were produced with high-throughput and had an average diameter of 60.5 µm with a polydispersity coefficient of 3.1 % and a symmetric lipid composition of both leaflets. The same devices was used to produce asymmetric GUVs using the "lipid in" approach, where the lipids are dispersed into the aqueous phases instead of into the oil phase (Karamdad et al., 2016).

Asymmetric GUVs were also produced with the microfluidic device developed by Lu et al. (2015). Four core steps composed the proposed approach : (1) forming highly uniform w/o emulsions in the oil/inner-leaflet-lipid solution that serve as precursors to form asymmetric vesicles based on the spontaneous assembly of lipid bilayers; (2) replacing the oil/ inner-leaflet-lipid solution that surrounds the w/o emulsions with the oil/outer-leaflet-lipid solution; (3) creating w/o/w double emulsions that encapsulate the w/o emulsion; and (4) extracting the trapped oil/outer-leaflet- lipid solution from the double emulsions (figure 9C). With this methodology, vesicles with a size ranging 20 to 120 µm can be obtained at a frequency up to 100 vesicles per second.

2.3.2. Water-in-oil-in-water w/o/w double emulsion

The w/o/w double emulsion method consists in generating w/o/w double emulsions with a coaxial microcapillary fluidic device that combines coflow- and flow-focusing geometries (Kamiya et al., 2017).

With this method, Deng, Yelleswarapu, et al. (2016) produced monodisperse uni- and multicompartment single bilayer liposomes (figure 11 A and B). By adjusting flow rates, they were able to monitor both the size of the vesicles ranging from 25 to 190 µm and the number of compartiments in multicompartment liposomes. In orther to extract the solvent present between the two lipid leaflet, a dewetting step was implemented to produce vesicles with undetectable amount of solvent. Due to interfacial energies, the solvent was spontaneously separated from the liposome (figure 11A, down). This process requires the same condition on interfacial tension as for the transfer of w/o emulsion droplets across a laminar interface

presented above. As the lipids were dissolved in the organic phase, the obtained vesicles had a symmetric composition of both leaflets.

The w/o/w double emulsion approach was also adopted by Deshpande et al. (2016) to develop an octanol-assisted liposome assembly (OLA) on chip (figure 11C). This approach uses octanol as the oil phase containing lipids and it allows the production of symmetric unilamellar vesicles with a size ranging from 5 to 20 µm. Again, a dewetting steps was achieved to separate the residual octanol from the liposome. In order to separate liposomes and octanol droplets generated during the dewetting steps, a density separation technique was developed to make the less dense 1-octanol droplets float to the top of a separation hole, while the liposomes were gently allowed to re-enter into the microfluidic channel (Deshpande et al., 2018).

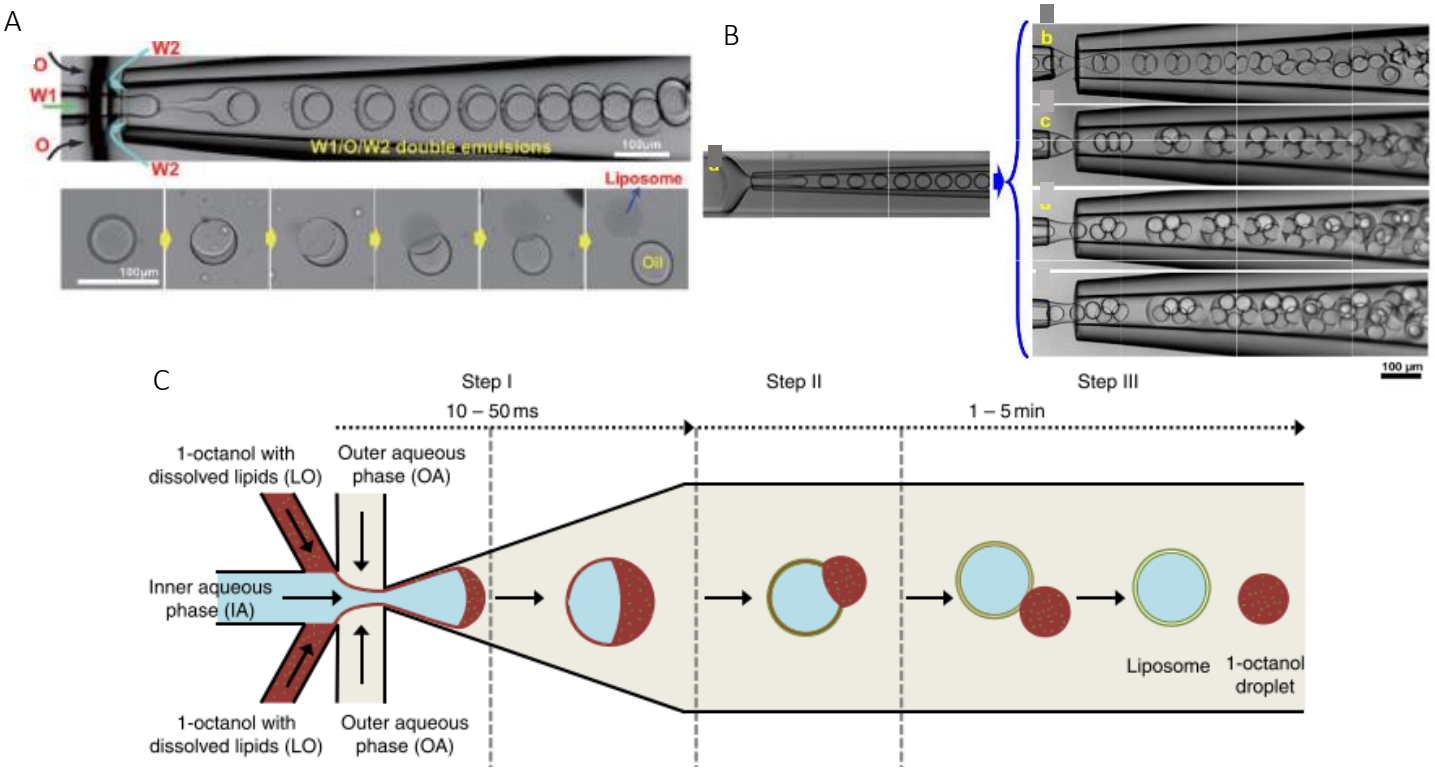

Figure 11 (A) Image of the giant liposomes formation device developed by Deng, Yelleswarapu, et al. (up) and the dewetting steps (down) (reprinted from Deng, Yelleswarapu, et al. (2016)) (B) Image of the multicompartment liposome formation developed Deng, Yelleswarapu, et al. (reprinted from Deng, Yelleswarapu, et al. (2016)) (C) Schematic of the octanol-assisted liposome assembly device developed by Deshpande et al. (reprinted from Deshpande et al. (2016))

2.3.3. Pulse jet flow

The third approach, the pulse jet flow technique, first developed by Funakoshi et al., mimics blowing of soap bubbles (Kei Funakoshi et al., 2007). Giant liposomes were generated by applying the pulsed jet flow

to a planar lipid bilayer. With this method, two types of monodisperse vesicles were obtained with size of 300 to 400 µm and 150 to 200 µm. However, some residual solvent was present in the lipid bilayer.
With the same approach, Kamiya et al. (2016) produced cell-sized vesicles. In a first steps, the pulse jet flow technique produced 2 types of vesicles having a size from 5 to 20 µm and 100-200 µm (figure 8C). The smaller vesicles contained less residual solvent compared to the bigger ones. As the presence of solvent makes vesicles unstable, the bigger vesicles collapsed rapidly and only the smaller vesicles remained. With this technique, asymmetric cell-sized vesicles were produced by forcing the flow throuhg an asymmetric planar lipid bilayer.

As shown in the previous paragraphs, the use of microfluidics to produce liposomes has become significantly investigated. Three approaches have been explored, each one having its specificity. The size of the produced liposomes is mainly over 1 µm. With flow-focusing devices, sub-micrometer droplets can be obtained by increasing the flow rate ratio (Φ), ratio between the flow of the inner and the outer phase (Jahn et al., 2007, 2010; Carugo et al., 2016).
Among the exposed methods, only two are able to synthetize vesicles with an asymmetric composition of lipids between leaflets. The w/o/w double emulsion may indeed show some difficulties to produce such asymmetry. Nevertheless, this method is able to produce liposomes with high throughput, so does the droplet emulsion transfer method. This high throughput is not achieved with the pulse jet flow approach as one experiment produces only about 20 vesicles (Kamiya et al., 2016). Finally, all techniques seem to be able to produce liposomes with a little amount of residual solvent in the lipid bilayer.

2.4. Liposomes to study interaction – Case study of surfactin

Lipid vesicles as GUVs, LUVs and SUVs have been used in several study to better understand the bioactive molecule-membrane interaction at microscopic and molecular scales. As shown previously in table 2, the use of several biophysical techniques to study the interactions between liposomes and target molecules can provide information on (i) their insertion and localization within a lipid bilayer (Nielsen et al., 2019), (ii)the thermodynamics of the bioactive molecules/lipids binding (Heerklotz et al., 2000), (iii) their effect on membrane stability/integrity (Heerklotz et al., 2004), and (iv) the effect on membrane dynamics (D'Auria et al., 2013).

The interaction of surfactins (SRF), a family of cyclic lipopeptides produced by *Bacillus sp*., with membrane models has been the subject of numerous biophysical studies in order to understand the molecular mechanism of their various biological activities. SRFs are a class of amphiphilic molecules formed by a ring-shaped heptapeptidic backbone closed by a β- hydroxy fatty acid (figure12) (Ongena et al., 2008). These molecules present a real scientific interest due to their antimycoplasma, antibacterial and antiviral properties (Huang et al., 2006; Ongena et al., 2007; Fira et al., 2018; Santos et al., 2018), their ability to stimulate plant defense response (Ongena et al., 2007, 2008; Pérez-García et al., 2011) and their potential health applications due to their antibacterial, anticancer and neuroprotective activity (Cao et al., 2010; Park et al., 2013; Santos et al., 2018). However, SRFs have limited antifungal activity (Ongena et al., 2007; Falardeau et al., 2013).

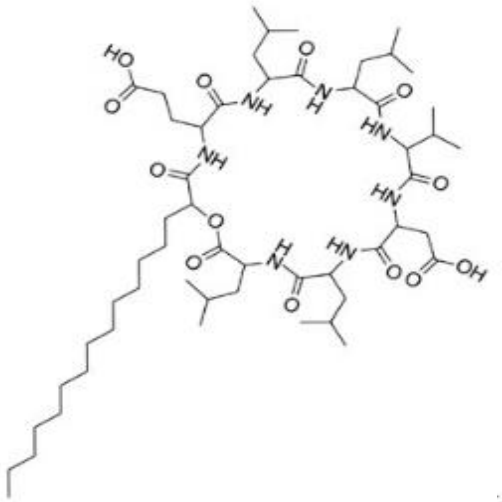

Figure 12 Molecular structure of surfactin (reprinted from Falardeau et al. (2013))

The biological activities of SRFs are highly supposed to be related to their interactions with the plasma membrane of target cells. The plasma membrane lipid composition variety of the target cell, illustrated in Table 1, could be at the origin of the specificity of SRFs interaction. The amphiphilic structure of SRFs is in favour of its insertion at a lipid interface via its fatty acid chain (Deleu et al., 2003; Henry et al., 2011). Such insertion of amphiphilic molecule into lipid vesicles has been correlated to antimicrobial activity (Hovakeemian et al., 2015). Besides, the SRF perception by plant cell has been suggested to be a lipid-driven process, due to its insertion into the lipid fraction of the plant PM, rather than a proteic receptor-driven mechanism involved in microbial associated molecular patterns (MAMPs) recognition (Henry et al., 2011). The insertion of SRF may disturb the lipid compartmentalization or induce curvature constraints in

host cell membranes which could lead to direct activation of mechanosensitive channels or proteins involved in signalling and the establishment of plant defense response (Henry et al., 2011). In addition, the structure of SRF has a key role in its perception. Small modifications in the peptide moeity lead to a significantly decreased defence-inducing activity and variations of the acyl chain length can either increase or hinder the SRF activity in tobacco cells (Henry et al., 2011).

The use of biophysical techniques combined with biomimetic models such as lipid vesicles and lipid bilayers is of crucial importance to decipher the mode of action of SRF at a molecular level.

These models can be very simple with only one type of lipids or more complex with several different lipids to mimic lipid domains and be closer to real biological membranes. The lipid composition of these models can also be adapted to mimick at best the studied organisms (Deleu et al., 2014). However, up to now, the studies of SRF were mainly done with biophysical models containing animal lipids such as POPC.

2.4.1. Insertion of surfactin into lipid bilayers

In the interaction process, one crucial step is the insertion/partition of the bioactive molecule from the external medium to the membrane. This insertion/partition can be described by thermodynamic parameters such as the variation of the free Gibbs energy informing about the spontaneity of the insertion, the variation of enthalpy and the variation of entropy giving rise to information about the nature of the interaction (electrostatic or hydrophobic), and the partition or binding constant corresponding to the affinity.

For SRF, a spontaneous entropy-driven insertion has been observed with POPC vesicles (Heerklotz et al., 2001; Razafindralambo et al., 2009; Henry et al., 2011), PLPC (palmitoyl linoleoyl phosphatidyl choline) vesicles (Henry et al., 2011) and mixed vesicles composed of PLPC/stigmasterol and DPPC (1,2-dipalmitoyl-sn-glycero-3-phosphocholine) /PLPC (Henry et al., 2011). This spontaneous insertion occurs with a high affinity of SRF for lipid bilayer as illustrated by the partition constant having a value ranging from 6.6 10^3 to 12.8 10^4 M^{-1} (Heerklotz et al., 2001; Carrillo et al., 2003; Razafindralambo et al., 2009; Henry et al., 2011).

The insertion of SRF is thought to be due to favorable van der Waals forces between the rather rigid cyclic and lipophilic part of SF and lipid chains (Buchoux et al., 2008). The binding affinity may vary with the membrane composition or the SRF structure. The presence of DPPC into the vesicles greatly increased K (Henry et al., 2011) while SRF variants with cyclic structure and a longer acyl chain length present a higher

affinity constant (Razafindralambo et al., 2009; Henry et al., 2011). However, the level of binding of PLPC vesicles was unaffected by the presence of stigmasterol (Henry et al., 2011).

2.4.2. Localization of surfactin into the lipid membrane and destabilization process

Another key information to better understand the mode of action of SRF is its localization into lipid membranes and how the insertion of SRF destabilizes membrane.

Based on zeta potential measurement, Fan et al. (2014) showed that SRF inserts exclusively into the outer leaflet at very low concentration (below 5 mol% of SRF in the membrane).This localization was also observed by Shen, Thomas, & Taylor (2010) and Shen, Thomas, Penfold, et al. (2010) who made neutron reflectometry on DPPC supported lipid bilayers. At higher concentration, a partial translocation of SRF into the inner leaflet was observed (Fan et al., 2014). Furthermore, Heerklotz et al. (2004) observed that this insertion promotes a tilt of the acyl chains and induces conformational change of the lipids with an increase in the wobbling motion of the $-P^{-}N^{+}$ dipole due to the electrostatic interaction of SRF with the lipid polar headgroups (Figure13). These elements suggest an insertion of SRF into the interfacial and upper hydrocarbon regions of the membrane. (Heerklotz et al., 2004).

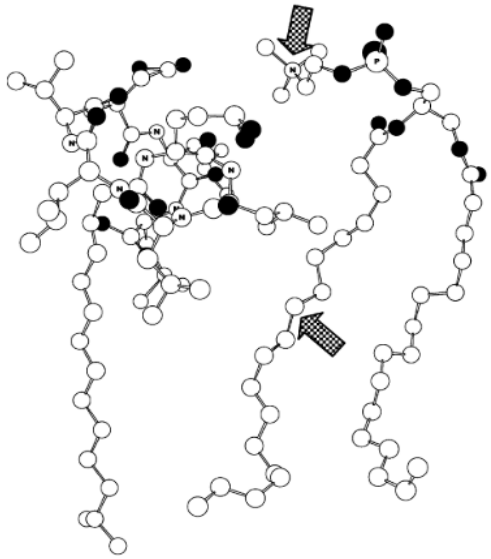

Figure 13 Schematic representation of the molecular dimensions and hypothetical localization of surfactin relative to the lipids in a membrane. Carbon atoms are shown in white, and oxygen, in black. Nitrogen, atoms are labeled with N, and phosphorus, with P. Hydrogens are omitted. Structural changes induced by SRF on the lipid conformation are illustrated with grey arrows (reprinted from Heerklotz et al. (2004))

Concerning the lateral localization of SRF, the presence of SRF-rich domains was observed into 1,2-dimyristoyl-sn-glycero-3-phosphocholine (DMPC) vesicles at a molar ratio of SRF of 1% to 2% mol (Grau et al., 1999). The presence of such domains into the bilayer was proposed to explain the increase of bilayer thickness observed (Grau et al., 1999). The properties of SRF molecule to self-aggregate into the lipid bilayer was also noticed by Carrillo *et al*. (2003) who suggested that SRF molecule self-assemble into the bilayer to form some type of oligomers, at least dimers or larger. These SRF oligomers may correspond to the ionic channels detected in presence of SRF in glyceryl monooleate bilayers (Sheppard et al., 1991) and DMPC supported bilayers (Liu et al., 2005). The distribution of SRF also appeared to be influenced by the presence of rigid domains into the membrane as SRF inserted at the boundary between gel and fluid lipid domains in DOPC/DPPC LUVs (Deleu et al., 2013).

In addition to the formation of pores, the asymmetric insertion of SRF in the outer leaflet would further destabilize the bilayer by an imbalance between the packing in the two membrane leaflets (Heerklotz et al., 2004). This imbalance in the bilayer showed the ability to induce leakage of calcein in POPC LUVs (Heerklotz et al., 2007). Two mechanisms are possible when leakage is observed in vesicles, namely all-or-none (i.e. some vesicles are fully leaked while others rest intact) or graded (i.e., all vesicles release part of the entrapped dye followed by an annealing of the membrane) mechanism. For SRF, a graded leakage mechanism was observed with POPC vesicles (Heerklotz et al., 2007; Patel et al., 2014).

As for the affinity, the lipid composition of the membrane can impact the rate of leakage or even the leakage mechanism following the insertion of SRF.

The presence of DPPC in POPC LUVs has shown to promote the SRF-induced leakage (Carrillo et al., 2003). This increase is in agreement with the increase of the affinity constant observed for DPPC/PLPC and could results in a higher affinity of SRF for rigid domains induced by the presence of DPPC LUVs (Henry et al., 2011).

The presence of sterols, such as Chol, seems to have a more complex effect. When measuring the initial rates of dye release, Chol reduced the rate of leakage (Carrillo et al., 2003; Oftedal et al., 2012) while no effect was observed when measuring the leakage after 1h of incubation (Fiedler et al., 2015). An explanation for these observation may come from the hypothesis of Hovakeemian et al. (2015) for the membrane disruption for detergent-like membrane permeabilizers such as SRF. This hypothesis suggests that detergent-like perturbation behaves in two phases, a fast but limited graded leakage, due to the asymmetric insertion of the active compound into the outer membrane leaflet, followed by a slow pore

formation (Hovakeemian et al., 2015). As the addition of Chol into vesicles has shown a shift from graded to all-or-none leakage, it implies that the second, slow effect becomes dominating in presence of Chol (Fiedler et al., 2015). Chol seems therefore to have an effect on the destabilization of the membrane and asymmetry stress by counteracting the positive membrane curvature induced by SRF (Carrillo et al., 2003; Heerklotz et al., 2007). As the first phase was argued to underlie the fast graded leakage, the initial rate of leakage is affected by the presence of Chol but not the long-term leakage (Fiedler et al., 2015).

The presence of POPE has shown to have an effect similar to the one observed with sterols. A decrease of the initial rate of leakage was observed in POPC/POPE LUVs (Carrillo et al., 2003) but only a small inhibition of long-term SRF-induced leakage for LUVs having similar lipid composition (Fiedler et al., 2015). The stabilizing effect of POPE against SRF leakage is thought to be linked to its counterbalancing effect on membrane curvature. The typical cone shape of PE counteracts the inverted cone shape of SRF (Carrillo et al., 2003). Therefore, POPE seems also to affect the fast phase of the leakage induced by membrane curvature stress due to the asymmetric insertion of SRF.

Finally, the presence of the negatively charged lipids 1-palmitoyl-2-oleoyl-sn-glycero-3-phosphatidylglycerol (POPG) in the LUV bilayers increased the long-term leakage and changed the leakage mechanism of SRF from graded toward all-or-none (Fiedler et al., 2015). The presence of negative charges on POPG could have been expected to decrease the binding of SRF which contains one negative charge at pH of 7.4. The increase of SRF activity has therefore been attributed to a stronger activity of membrane-bound SRF. The electrostatic repulsions increase head-head distances, enhancing the positive intrinsic curvature of the molecules, and reduce the energetic cost of segregating charged molecules for more localized action such as pore formation (Fiedler et al., 2015). Such impact of the lipid charge has also been observed in DMPC/DMPS SUVs where SRF destabilized vesicles only when the serine group was negatively charged (i.e. at pH 7.5) (Buchoux et al., 2008).

2.4.3. Impact of surfactin on lipid bilayer organization and properties

Before the solubilization of the lipid bilayer by the SRF, the presence of SRF into the membrane affects its organization and properties such as the membrane ionic permeability and membrane order and fluidity.

The change in membrane ionic permeability seems obvious since SRF is thought to form ionic channel into the membrane (Sheppard et al., 1991; Liu et al., 2005). This hypothesis was suggested with the observation

of an increase of glyceryl monooleate bilayers cationic conductance in presence of SRF (Sheppard et al., 1991) and supported with a cyclic voltammetry experiment on DMPC supported bilayers (Liu et al., 2005).

Concerning the membrane order, SRF was found to interact with both the membrane acyl chain and the polar heads regions (Carrillo et al., 2003; Heerklotz et al., 2007; Deleu et al., 2013). In POPC MLVs, the SRF interaction with the polar head region induced a strong dehydration resulting in a lower water penetration in this region, while the strong interaction with the acyl chains resulted in a net fluidizing effect of the apolar part of the bilayer (Carrillo et al., 2003). These results are consistent with another study made on DOPC/DPPC LUVs where it was evidenced that, at a concentration close to the CMC, SRF increased the membrane order due to the solubilization of the DOPC fluid phase, favoring the presence of only one DPPC rigid phase (Deleu et al., 2013).

Another membrane property which is affected by the presence of SRF is its lateral organization. Indeed, in living human red blood cells, SRF increased the formation of some BODIPY (boron dipyrromethen) fluorescent lipid (sub)micrometer domains at concentration well below the CMC (D'Auria et al., 2013). In opposite, in DOPC/DPPC LUVs, SRF eroded the DPPC rigid domains at a concentration below its CMC (Deleu et al. 2013). However DPPC domains remain intact at a concentration close to the CMC. These findings suggest that the effect of SRF on lipid lateral organization may be dependent of the SRF concentration, as it is the case for the different phases of the SRF-induced membrane destabilization.

2.4.4. The concentration-dependent effect of SRF on membrane

In the mechanism of membrane destabilization, the increase SRF concentration along the process showed the appearance of several delimited stages as illustrated by the different proposed models.
For the leakage of POPC membrane, Heerklotz et al. (2007) found that the leakage starts at a surfactin-to-lipid ratio in the membrane, Rb ≈ 0.05 with a graded leakage due to the curvature stress induced by the insertion of SRF into the outer leaflet which produces transient membrane failure followed by a membrane annealing. When Rb reach a value of ≈ 0.15, the permeabilization behavior switch to a leakage where all dye can leak out from the vesicles after sufficient time. At this phase, the presence of SRF-rich clusters allows a leak that is stabilized by a SRF-rich rim covering its edge. Finally when Rb reaches a value of 0.22, membrane lysis or solubilization begins and mixed micelles containing SRF and solubilized lipids are formed. This solubilization is complete at a SRF-to-lipid ratio of 0.43.

With DMPC vesicles, a similar SRF solubilization model was proposed by Kell et al. (2007) with three different aggregation forms. At low SRF-to-lipid ratio until 4 mol%, vesicular particles were observed, some of them having a lateral phase separation with SRF-rich domain. Between 4–15 mol% of SRF, the DMPC-vesicles were progressively disrupted into sheet-like lamellar membrane fragments with a length of 50–100 nm and a width of 4–5 nm, where lipid-rich and SRF-rich domains presumably alternate with each other within the bilayer membrane. Above 15 mol% of SRF, smaller (<10nm) ellipsoidal particles were formed which presumably represent mixed micelles of DMPC and SRF (Kell et al., 2007).

With mixed supported bilayers composed of DPPC and SRF, Shen, Thomas, & Taylor (2010) also reported an effect of SRF concentration. If SRF concentration was above its CMC either during the bilayer deposition or after its deposition, the bilayer either did not deposit or was removed, respectively. Further investigation of the SRF localization within lipid bilayers during the solubilization process showed that the process involved, first, a penetration of SRF into the outer leaflet, formation of SRF auto-aggregate, followed by a solubilization of the bilayer when the SRF concentration reached a threshold concentration (i.e. its CMC) (Shen, Thomas, Penfold, et al., 2010).

For the solubilization of DOPC/DPPC membranes, which display a phase separation, another model with three sequential structural and morphological changes was proposed by Deleu et al. (2013). At a concentration below the CMC, SRF inserts at the boundary between DPPC rigid domains and DOPC. As the concentration of SRF is increased close to CMC (15 µM at 25° C) an immediate solubilization of the fluid phase occurs but DPPC rigid domain remains. At this step, mixed micelles and bilayered disk-like structures appear. When the concentration of SRF is higher than the CMC, a total destabilization of the lipid bilayer occurs with a direct formation of mixed DOPC- and/or DPPC-SRF micelles as well as large particles resulting from mixed micelles organized in a large network assembly and/or remodeled fluid supramolecular entities with diverse morphologies (Deleu et al., 2013).

Even though all the presented models have different concentration thresholds between the membrane destabilization stages, all of them seem to agree in a SRF mechanism composed of three to four main phases. At low SRF concentration, SRF inserts into the membrane and can induce a partial membrane destabilization due to an asymmetric curvature stress followed by a membrane annealing process in a first step. At medium SRF concentration into the lipid bilayers, the formation of SRF clusters occurs within the membrane and stabilizes the membrane leakage.

When the SRF concentration further increases, it reaches a threshold where the membrane solubilization begins. This solubilization starts with the appearance of mixed micelles and bilayered disk-like structure containing a mixture of SRF and solubilized lipids. Finally, at high SRF concentration, the solubilization is complete with the presence of only mixed micelles and larger entities resulting from mixed micelles organized in a large network assembly and/or remodeled fluid supramolecular entities with diverse morphologies.

The precise concentration separating each step is not clearly established and may vary with the lipid composition and the presence of lipid domains in the membrane as the SRF membrane affinity has shown to be sensitive to these parameters.

2.4.5. Importance of surfactin structure for bilayer disturbance

Through the previous sections, it was shown that the effect of SRF on membranes was clearly affected by its lipid composition and the SRF concentration. Nevertheless, the SRF structure has also a key role in membrane disturbance, as illustrated by the variation of biological activities within the SRF variants. Three structural characteristics are implicated: the cyclic structure of the peptide part, the acyl chain length and the electric charges.

When the peptide moiety of SRF does not present a cyclic structure, a complete loss of burst-inducing activity was observed in tobacco cells (Henry et al., 2011) as well as a loss of hemolytic activity on red blood cells (Dufour et al., 2005).

Concerning the acyl chain length, a chain shorter than 14 and 15 carbons leads to the complete loss of SRF activity on tobacco cells (Henry et al., 2011). A direct correlation with the acyl chain length was also observed for SRF antiviral and hemolytic (Kracht et al., 1999; Dufour et al., 2005).

The SRF charge was reported to influence the SRF hemolytic (Dufour et al., 2005) and antiviral activities (Kracht et al., 1999). In the first case, the presence of third negative charges in SRF reduced slightly its hemolytic activity compared to the SRF variant having only two negative charges. In the second case, the absence of negative charge inhibits antiviral activity.

The effect of these three structural parameters was also observed with biomimetic models. In DOPC/DPPC supported bilayers, the absence of the cyclic structure of the peptide has led to an important decrease in SRF membrane interaction activity. While the natural cyclic SF solubilized both DOPC and DPPC, its linear

SRF with the same acyl chain length, solubilized DPPC more slowly and induced redeposition of SRF/ phospholipid material, leading to a newly formed homogenous bilayer (Francius et al., 2008). The loss of the cyclic structure was also reported to reduce significantly the binding affinity of SRF for POPC vesicles (Razafindralambo et al., 2009). One possible explanation is that the linear variant of SRF has a lower hindrance of the head group and consequently a lower tendency to disrupt membranes (Dufour et al., 2005).

The study of Francius *et al.* (2008) also illustrated the importance of acyl chain length. While the linear SRF variant with an acyl chain of 14 C has a much lower activity on DOPC/DPPC supported bilayer than the cyclic variant, the linear variant with 18 C kept a similar behavior than the cyclic variant. This suggests that the increase of the chain length compensated the loss of the peptide cycle due to stronger hydrophobic forces with the longer acyl chain length (Francius et al., 2008). In opposite, the linear variant with a chain length of 10 C showed poor membrane activity on DOPC/DPPC supported bilayer with no alteration of the surface topology. Such impacts of the acyl chain length were also observed on the binding affinity of SR variant with plant root cell membrane model and POPC vesicles (Razafindralambo et al., 2009; Henry et al., 2011). Finally, the charges of SRF also showed an influence on the SRF interaction with membrane models. They influenced the electrostatic repulsions between molecules which has a role in membrane disturbance (Buchoux et al., 2008). SRF contains two acidic residues, a L-glutamic and a L-aspartic, and its pK value at the water-air interface has been evaluated to be ≈ 6 (Maget-Dana et al., 1992). The deprotonation of these residues can influence the interaction of SRF with lipid membrane and particularly in presence of calcium ions. Grau et al. (1999) showed that the presence of Ca^{2+} cation at pH 8.5 resulted in a stronger effect of SRF on DMPG vesicles but this was not observed at pH 7.4 and 5.5. These results suggest that the SRF molecule is still essentially protonated at pH 7.4. In addition, when the SRF is deprotonated (i.e. at pH 8.5), the effect of the presence of Ca^{2+} observed is in agreement with the formation of a SRF- Ca^{2+} (1:1) complex which is expected to be located more deeply into the bilayer, resulting in a stronger SRF interaction (Thimon et al., 1992; Grau et al., 1999). However, the influence of SRF charges may depend on the membrane composition. When comparing the activity of a SRF linear variant with 2 negative charges and one having the same acyl chain length and 3 negative charges, Francius et al. (2008) observed a lower membrane activity on DOPC/DPPC supported bilayer for the one having two negative charges. The latter was not able to solubilize DPPC contrary to its more negative homologue.

In conclusion, the use of liposomes and lipid bilayers as biomimetic models has given important information about the SRF behavior towards lipid membranes, which can give valuable insights about the molecular mechanism involved in the biological activities of SRF.

The SRF mechanism is influenced by the lipid composition of the bilayer, the SRF concentration, and the structure of SRF. It starts by the spontaneous insertion of SRF into the outer leaflet of the lipid bilayer which induces curvature stress and electrostatic repulsion due to the hindrance and the negative charges of the peptidic head of SRF. When the concentration of SRF in the membrane increases, SRF-rich domains are observed and can form pore through the membrane. During these two phases the presence of SRF may also alter the lateral lipid distribution of lipids by favoring or suppressing lipid domains. At higher SRF concentration, the membrane becomes solubilized into membrane fragments and mixed micelles.

3. Objectives and strategy of this thesis

Through the previous section, the importance of the lipid fraction of the PM in various biological mechanisms has been highlighted. The intricate organization of the PM containing more than one hundred lipids has driven researchers to develop simplified model systems to decipher the mechanisms at the molecular level. One of them is the liposome, or lipid vesicle, which is a lipid bilayer that surrounds an aqueous droplet.

Liposomes can be made of one or two different kind of lipids for fundamental biophysical studies. A higher number of lipids can be used to better mimic biological systems. But the importance of the lipid asymmetry between the outer and the inner leaflet was only little considered while it is known that is crucial for the normal functioning of living cells. However biomimetic models having an asymmetric lipid composition between leaflets were only developed in the last few years. Techniques using microfluidics or cyclodextrin catalyzed exchange are under investigation to produce asymmetric liposomes. Up to now, very simple compositions using conventional lipids are considered. No study has focused on forming asymmetric liposomes mimicking plant plasma membranes.

The present thesis aimed at developing a microfluidic device to form asymmetric liposomes in a reproducible manner and with a minimum of steps.

A critical point in this process is the elimination of the residual solvent used to perform the assembly of the two leaflets of the bilayer. Some previously reported techniques using microfluidics to form liposomes either used a time-consuming step to extract the solvent from the liposome (Lu et al., 2015) or could not avoid the presence of residual solvent droplets alongside the liposomes (Deshpande et al., 2018). To extract more easily the solvent, the approach suggested by Deng, Wang, et al. (2016) using the spontaneous transfer of w/o emulsion droplets across a laminar interface will be explored.

To achieve the asymmetry between leaflets, the approach of inverted emulsion transfer will be used as previously reported for asymmetric liposome production (Lu et al., 2015; Karamdad et al., 2016). In this way, each leaflet will be created separately before the liposome formation in order to get a control on their composition.

The design of the chip will therefore have two different junctions to create the inner leaflet first and then the second leaflet. For the production of the chip, a point of attention will be the hydrophilic modification of the channel after the second junction in order to avoid the wetting of the channel wall by the liposome

(Karamdad et al., 2015; Lu et al., 2015; Deshpande et al., 2016). To achieve such modification, polyvinyl alcohol (PVA) will used as previously proposed (Deshpande et al., 2016; Trantidou et al., 2017).

In a short-term, the goal of the microfluidic device is to produce biomimetic asymmetric liposome containing plant lipids. Such plant plasma membrane models could be used with biophysical techniques to study the interaction of plant eliciting molecules, like surfactin, with plant PM in order to get novel insight about the molecular mechanism of its recognition by plant cell, one crucial step in its eliciting activity. Moreover, by developing more realistic plant biomimetic PMs, the project will also provide new perspectives for the fundamental understanding of their structural organization.

4. Development of the experimental setup

4.1. Chip design

The global design of the chip developed in this work to generate lipid vesicles is illustrated in figure 14. This design is made in order to perform a two steps assembly of liposomes with the successive formation of the inner and the outer leaflets. In the first step, some w/o emulsion is generated at a flow-focusing junction, where the inner aqueous phase containing lipids (W1) is sheared by octanol (figure 14 a). The resulting W1

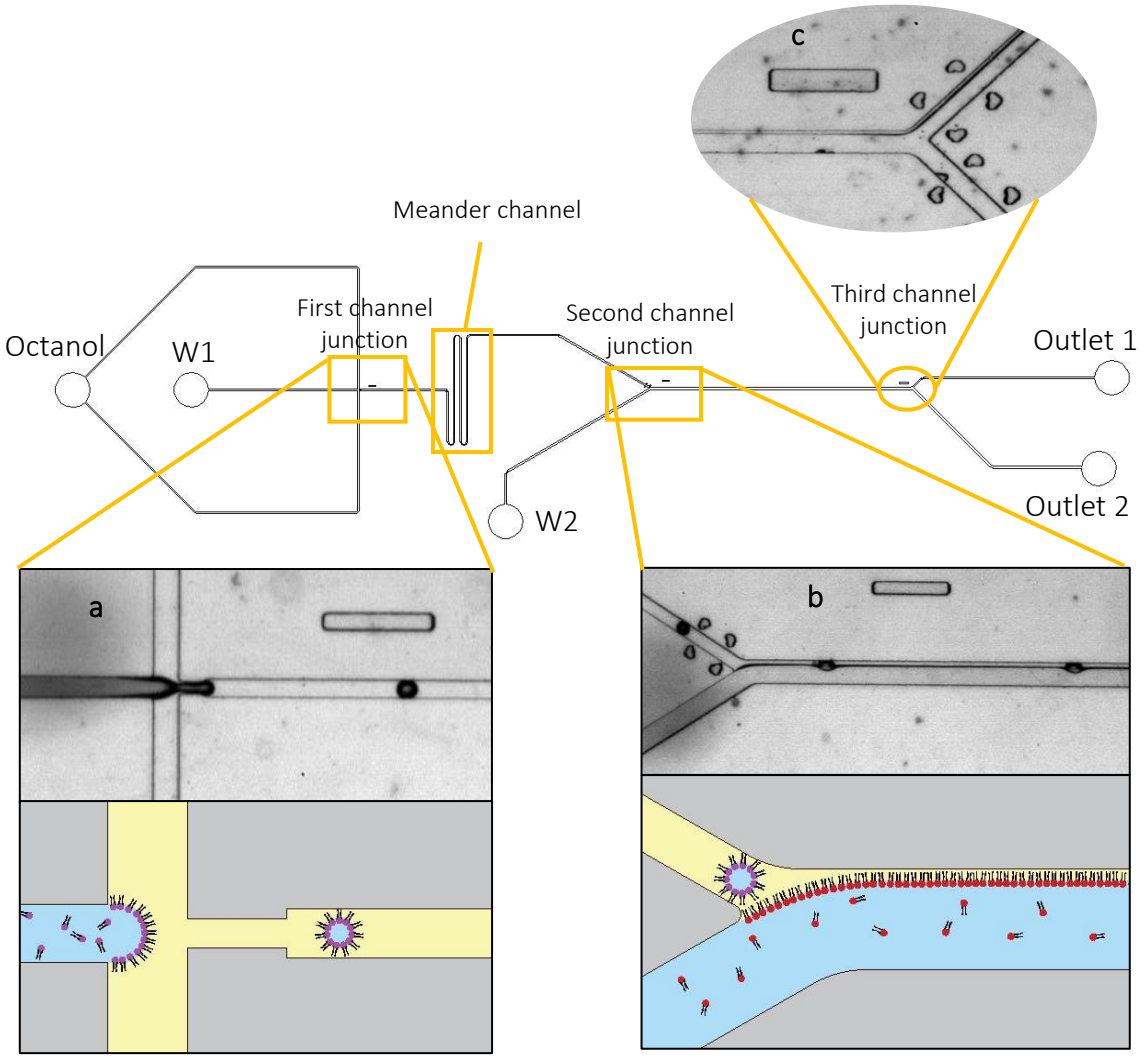

Figure 14 Schematic and bright-field images of the chip design used. (a)Image of the flow focusing junction where the W1 phase containing lipids is sheared by the octanol phase to produce w/o emulsion (scale bar = 416 µm). (b) Image of the co-flow of the w/o emulsion and the W2 phase when the channel is partially coated with PVA (scale bar = 416 µm). (c) Image of the separation into two outlet channels, the upper contains the octanol phase and some W2 phase and the bottom channel contains only W2 phase (scale bar = 500 µm).

droplets dispersed into the octanol phase are stabilized with the lipids contained in W1, which will spontaneously form a monolayer surrounding the droplets constituting the inner leaflet of the liposome. The emulsion then flows through a meander channel prior to meeting the outer aqueous phase containing dispersed lipids (W2). This meander provides enough time for the lipid to self-assemble into a monolayer. It also increases the hydrodynamic resistance between the two junctions which renders the production of the W1 droplets more independent from the inlet pressure of W2. When reaching the second junction, the droplets surrounded by a lipid monolayer meet a second interface where a second lipid monolayer is formed with the lipids contained into W2 (figure 14 b). At this second step, both monolayers can be assembled to form a liposome. Finally, a third junction is added in the design in order to perform a separation between the octanol phase and W2 containing the formed liposomes (figure 14 c).

As the generated liposomes would be used as a biomimetic model of the plasma membrane, their size should be close to the size of living cells (i.e. several µm). To achieve such small-sized liposome, the choice of the channel size (height and width) is important as it impacts the size of the produced droplets. This size is also limited by the microfabrication resolution (channel width smaller than 30 µm was not accessible) and the risk of leakage at inlets for chips with a relatively high hydrodynamic resistance, i.e. with small channel width and height.

The channels height is set at 50 µm to get small droplets but avoid too resistive channel. The width of the channel was set at 30 µm in the shrinkage at the exit of the flow focusing junction to decrease the size of W1 droplet. The other dimensions (width and length) of each channel are presented in table 3.

Table 3 Width and length of each channel of the chip used

Channel	Width (µm)	Length (µm)
1	65	8500
2	85	25350
3	65 (30 at the shrinkage)	38150
4	95	11250
5	110	10000
6	85	10550
7	85	11400

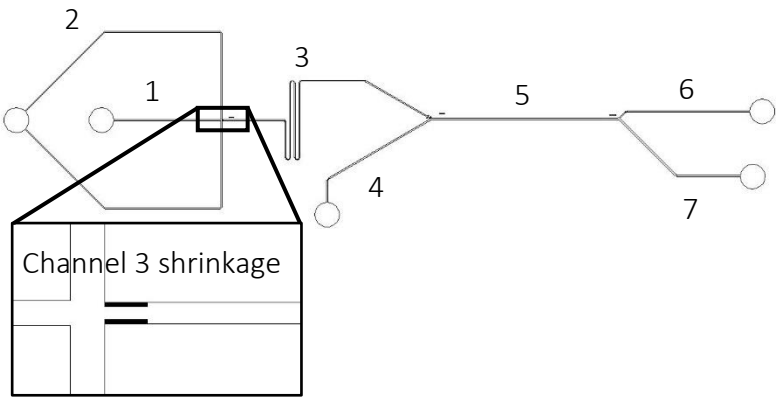

4.2. PVA treatment

Besides the design of the chip, the hydrophilic modification of the channels following the second junction was another key point to obtain a chip able to produce liposomes. Such modification has been reported to be necessary to avoid the wetting of the droplets to the hydrophobic channel surface of PDMS (Karamdad et al., 2015; Lu et al., 2015; Deshpande et al., 2016). Indeed, without the treatment, the droplet containing the W1 phase would directly merge with the W2 phase when reaching the second junction (figure 15).To perform the hydrophilic treatment, polyvinyl alcohol (PVA) was used.

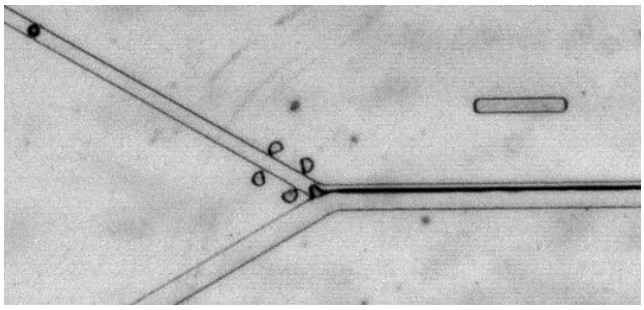

Figure 15 Fusion of a W1 droplet with the W2 phase in a PDMS channel without hydrophilic treatment

To achieve an efficient PVA treatment of the channel, attention must be paid to the concentration of the PVA solution used, the elimination of PVA residue in the channel prior to fixing thermally the adsorbed PVA and the time between the plasma exposure and the treatment.

The concentration of PVA must be high enough to have a sufficient adsorption of PVA, although a too high concentration leads to the presence of PVA agglomerates that could clog the chip channel. During the experiments, a concentration of 2.5 % (w/w) of PVA was found to be suitable for the treatment with a filtration step through a syringe filter of 0.2 µm pore size to eliminate any PVA agglomerates.

The concentration may also affect the elimination of PVA residues prior to the baking of the treated chip to fix thermally the adsorbed PVA. This elimination is important as any remaining PVA droplet would form a clog into the channel after the baking. As a higher PVA concentration leads to a higher solution viscosity (Ōyanagi et al., 1962), the elimination of a more concentrated solution is more difficult.

A PVA treatment right after the plasma exposure leads to a trickier control on fluids flow (i.e. entry of PVA into the wrong channel occurs more often) while a treatment significantly later than the exposure did not allow the modification of hydrophilicity. The adsorption of PVA onto the PDMS surface is indeed due to the presence of alcoholic hydroxyls (C–OH), silanols (Si–OH), and carboxylic acids (COOH), introduced during plasma exposure, which allows hydrogen bonding between the PVA molecules and the activated PDMS

surfaces (Wu et al., 2005; Trantidou et al., 2017). The presence of these polar groups at the surface of PDMS decreases with time after the plasma exposure due to their reorientation from the surface to the bulk, so the hydrophilic effect of plasma treatment on the PDMS surface may disappear within a day (Tan et al., 2010). A resting period of four hours to an overnight between the plasma exposure and the PVA treatment was found to be adequate to control fluids flow and get an effective hydrophilicity modification.

Based on all these considerations, the treatment was realized by passing a solution of 2.5% w/w of PVA through the adequate channels for about 10 minutes. The channels were then dry by flushing air to eliminate any residual droplet of PVA in the channels. The chip was then baked at 120 °C for 10 minutes to fix the PVA to the channel walls.

The PVA treatment was shown to significantly decrease the hydrophobicity of PDMS, thereby reducing the water contact angle of PDMS from above 100° to below 40° (Trantidou et al., 2017). However, such treatment has also the ability to invert a w/o emulsion into an o/w (figure 16) and therefore, the channel preceding the second junction, containing the w/o emulsion, has to be preserved from the PVA. To modify the hydrophobicity of the channel following the second junction only, the PVA solution was injected through the W2 inlet while a positive air pressure was applied through the W1 and the octanol inlets. To completely coat the channel, an air pressure of about 250 mbar was applied on the W1 and the octanol inlet and the PVA solution was injected with a pressure of 320 mbar then increased gradually to about 385 mbar.

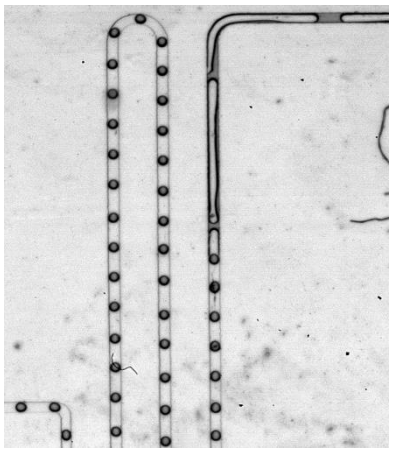

Figure 16 Image of an inversion of w/o emulsion into o/w emulsion

5. Materials and imaging for the production of liposomes

5.1. Preparation of lipid dispersions and PVA solution

To prepare the aqueous phases, egg phosphatidylcholine (egg PC, sigma Aldrich) was first dissolved into a mixture of chloroform:methanol (2:1, v:v) in a round bottomed flask. The solvent was evaporated under vacuum (Rotavapor R Buchi RE-111, Buchi, Flawil, Switzerland) to obtain a thin lipid film that was dried overnight in a vacuum desiccator to remove remaining solvent. The dry lipid film was then hydrated with the desired amount of Tris(hydroxymethyl)aminomethane - HCl (Tris-HCl, sigma Aldrich) 10 mM buffer at pH 7.4 for 1h at 40 °C and shaken every 10 minutes. This step disperses lipids in the form of lipids multilamellar vesicles into the buffer. The lipid final lipid concentration was 7.5 mg/mL. The mixture was then dissolved with Tris-HCl buffer to make a 3 mg/mL lipid solution (used as outer aqueous phase, W2) or with a blue dye solution to make a 5 mg/mL lipid solution (used as inner aqueous phase, W1).

To get a homogenous dispersion of lipids vesicles and a unilamellar form, the multilamellar vesicles were either extruded or sonicated. For the extrusion, before the dissolution of the 7.5 mg/mL solution, the vesicles were subjected to 5 freeze-thaw cycles, with liquid nitrogen and a water bath at 40°C, prior being extruded 11 times through 0.1 µm membrane filter. For the sonication, both the W2 and the W1 solutions were sonicated for 10 minutes, 3 times, in an ultrasonic cleaner (USC 300TH, vwr™). As long as the lipid dispersion was homogenous, the same results were obtained with both extruded and sonicated lipid vesicles.

The PVA solution was prepared by adding PVA powder (average molecular weight 145000, ≥98% hydrolyzed, Merck) into de-ionized water to reach a concentration of 2.5 % w/w. The mixture was then heated until boiling and kept boiling for 40 minutes with a manual stirring. After that, the mixture was weighted and de-ionized water was added to compensate the loss of evaporated water. The obtained solution was passed through a 0.2 µm syringe filter prior the injection into the chip in order to avoid remaining PVA clogs in the solution which could block the channel of the chip.

5.2. Soft lithography

Microfluidic chips were fabricated in polydimethyl siloxane (PDMS) by soft lithography (figure 17)(Mazutis et al., 2013; van Loo et al., 2016). First, the design of the mask was drawn in AutoCAD (AutoDesk) and printed on a foil mask with a photoplotter (Bungard, resolution 8192 dpi). Then a master was fabricated by

spin coating and locally exposing the layer (red layer in figure 17) of SU-8 negative photoresist, a light sensitive material, (SU-8 2050, MicroChem, MicroResist Technology) to UV on a silicon wafer with a targeted thickness of 50 µm (figure 17, step1). The master was silanized for 3 h in a desiccator in order to prevent the replica from sticking to the master. The PDMS chip were then fabricated by pouring a degassed mixture of Sylgard 184 PDMS prepolymer and curing agent (Dow Corning) in a ratio 10:1 onto the master and baking it for 45 minutes at 85°C (figure 17, step2) to insure the PDMS cross-linkage. After that, the cured PDMS was thoroughly peeled and the inlets/outlets holes were punched (figure 17, step3). In parallel, microscope glass slides were spin-coated with a very thin layer of PDMS and cured at 85°C for 30 min. Finally, the PDMS chip was bound to these PDMS- coated glass slides after plasma activation (air plasma, Diener, 60 s) and baked for 45 minutes at 85 °C (figure 17, step4) to insure the binding between the PDMS and the glass slides, prior the PVA treatment of the channel (see section 3.2.).

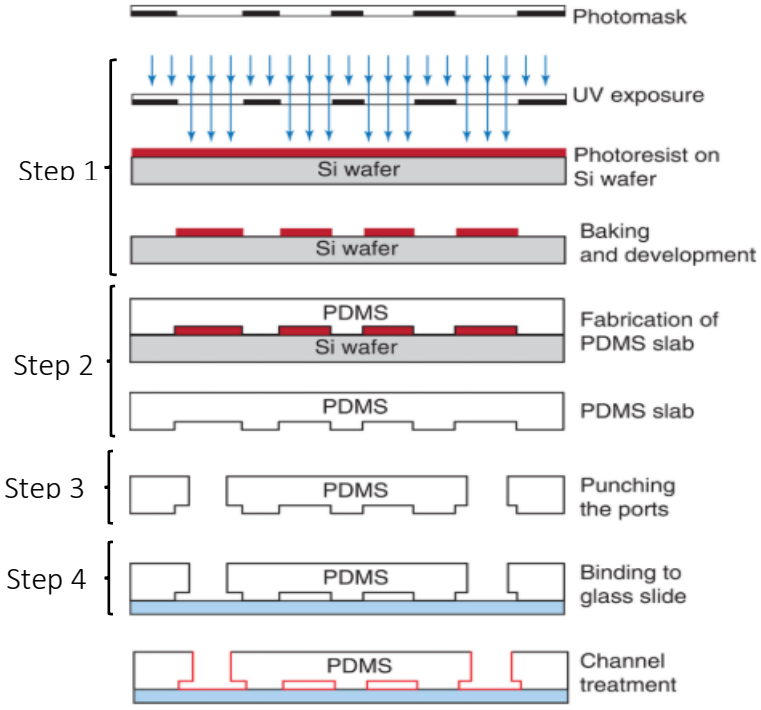

Figure 17 Different steps of microfluidic chip fabrication by soft-lithography (adapted from Mazutis et al.(2013))

5.3. Operation with the microfluidic chip

For producing liposomes with the microfluidic chip, egg PC solutions and 1-octanol (sigma Aldrich) were injected into the microfluidic device with a microfluidic flow control system (MFCS™-EZ, Fluigent) connected with PVC tubing (Thermo Scientific) with an inner diameter d_i=1mm, an outer diameter d_o=2mm, length L_t=0.1m, and a Young's Modulus E_t=6.1MPa.

5.4. Imaging and measurement

Image were captured using stereo-microscope (Zeiss SteREO Discovery.V12) combined with a high-speed camera (Photron Fastcam MINI UX100). Video processing and subsequent quantitative analysis were performed using ImageJ and a dedicated MATLAB script.

A representation of the measurement realized with the script is shown in figure 18. Briefly, the diameter of both W1 and liposomes (and also octanols droplets) was estimated from the volume of the droplet (diameter = $(6V_d/\pi)^{1/3}$). This volume was calculated using the approximation of van Steijn et al. (2010):

$$V_d = H * A - \frac{H^2}{2} * \left(1 - \frac{\pi}{4}\right) * l$$

Where V_d is the volume of the droplet, H is the height of the channel (50 µm in this case), A is the top-view area and *l* is the perimeter of the droplet.

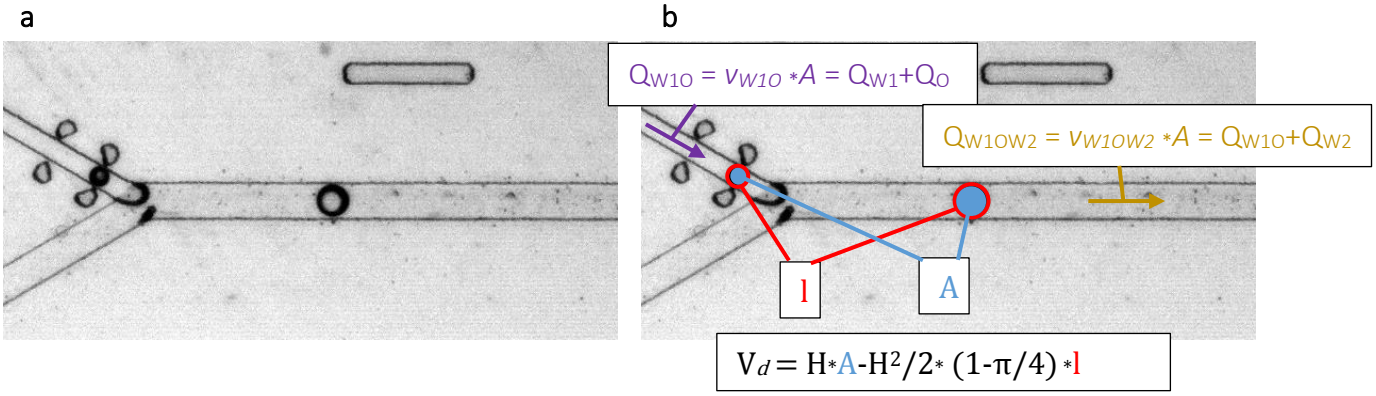

Figure 18 Illustration of the image analysis performed with the MATLAB script. (a) Original image. (b) Measurement realized with the script (see text for the meaning of each term)

The total flow rates of the channel containing liposomes, Q_{W1OW2}, and W1/o emulsion, Q_{W1O}, were determined with the relation $Q = v * A$, where Q is the flow rate, v is the fluid velocity and A is the cross-sectional area of the channel. The fluid velocity was assumed to be the same as the droplet velocity (Jakiela et al., 2011). The subtraction of these two flow rates gave the flow rate of the outer aqueous phase, Q_{W2}. The flow rate of W1, Q_{W1}, was obtained by measuring the proportion of the W1 phase into the channel containing the W1/o emulsion (S_{W1}/S_{W1O}) and multiplying Q_{WO} by this proportion ($Q_{W1} = Q_{W1O} * S_{W1}/S_{W1O}$). The flow rate of the octanol phase, Q_O, was obtained by subtracting Q_{WO} and Q_{W1}. All these information were collected at the second channel junction of the chip and used to discuss the influence of these parameters on the liposome formation (see section 6.3.).

6. Production of liposomes

6.1. Choice of the lipids and the organic phase

Next to the design of the chip, another important choice is the composition of the different phases. As the final objective is to produce asymmetric vesicles, the lipids were dissolved into the two aqueous phases to avoid the mixing of these lipids. Octanol was used as organic phase as Deshpande et al. (2016) have shown its ability to spontaneously bud from liposomes, allowing the production of liposomes containing little residual octanol. In this work, the chosen lipids were egg phosphatidylcholine (egg PC) for both aqueous phases as it is a cheap lipid already used for the production of liposomes (Deng, Yelleswarapu, et al., 2016), therefore interesting for the phase of development of the device. Furthermore, as illustrated in table 1 in the introduction (section 2.1.1.), PC is one of the main lipids of biological plasma membranes.

The aqueous phases were prepared by dispersing the lipids as small vesicles with a conventional protocol (see chapter 5.1.). This kind of dispersion allows a stable and homogenous repartition of the lipids into each phase (W1 and W2).

6.2. Production of liposomes with the microfluidic chip

Two different approaches were considered: the spontaneous transfer across laminar interface suggested by Deng et al. (2016) and the droplet emulsion transfer approach (Karamdad et al., 2015; Lu et al., 2015). In the case of the droplet emulsion transfer, the PVA treatment of the channel following the second junction was applied to the whole channel (figure 19 a). For the transfer across laminar interface approach, the upper wall of the channel (the wall on the side of the entrance of the w/o emulsion) was preserved from the PVA (figure19 b).

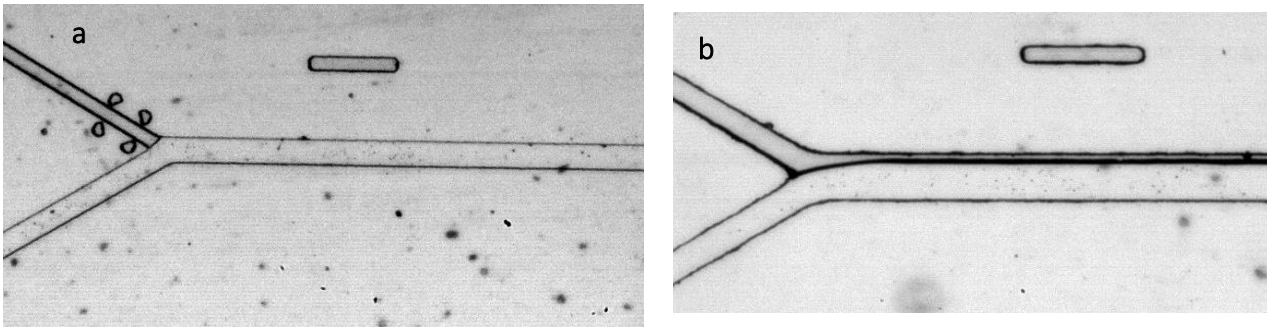

Figure 19 Image of the realization of the PVA treatment for (a) the droplet emulsion transfer and (b) the transfer across laminar interface approach

The method of spontaneous transfer across laminar interface was explored in order to separate easily the oil phase from the water phase containing the liposomes. Indeed, with this technique, a co-flow of the w/o emulsion and the W2 phase will be observed and the liposome will be formed when the W1 droplets cross the interface and migrate into the W2 phase. After the transfer, we would get the W2 phase containing the liposomes on one side of the channel and the octanol phase on the other side. The two phases may then be collected separately using the Y-junction illustrated in figure15c. All these steps are illustrated in figure 20.

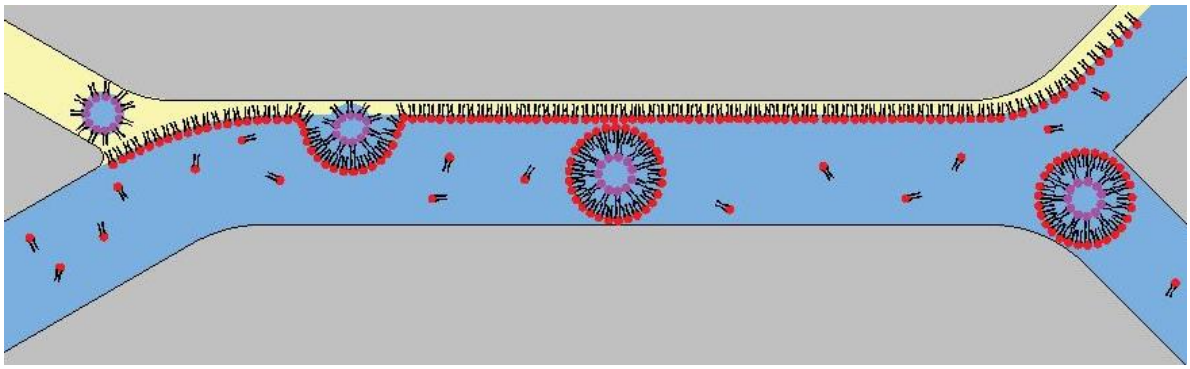

Figure 20 Schematic representation of the transfer spontaneous across laminar interface methodology

However, the experimental results obtained with this approach were different than the expectation. When the water droplet reached the interface, it burst which did not allow the liposome formation (Figure 21). Two reasons may explain the results : the difference of viscosity between octanol (7.288 mPa.s at 25°C) and water (0.89 mPa.s at 25°C) or the presence of an osmotic stress.

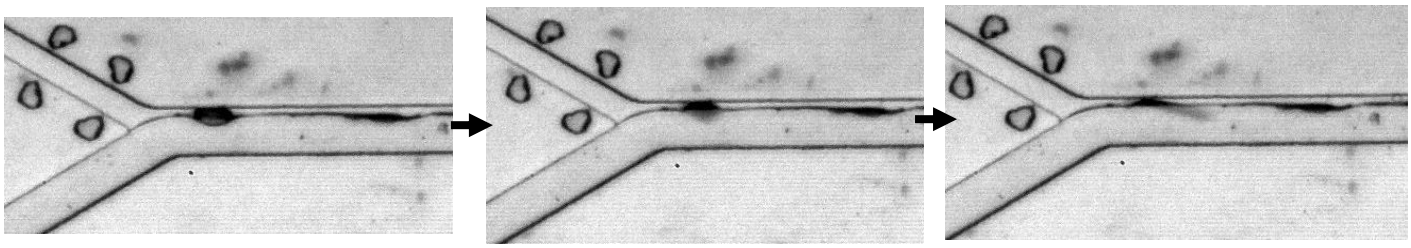

Figure 21 Droplet burst observed with the transfer across laminar interface approach

In the first hypothesis, the difference of viscosity involves a difference in fluids velocities (Guillot et al., 2006) that could have destabilized the lipid organization at the interface between the W1 droplets and the W2 phase, inducing the fusion of the droplets with the W2 phase. This difference in fluid viscosities was much lower in the experiment of Deng, Wang, et al. (2016) who produced polymerisome with this method using a mixture of chloroform and hexane (38:62, v/v) instead of octanol and an aqueous solution with 10% of PVA as W2 phase.

With the osmotic stress hypothesis, an imbalance between the osmotic pressure of the W1 phase and the W2 phase could have produced a vulnerable system, inducing the droplet burst (Gao et al., 2009). Such osmotic pressure imbalance has already been reported to influence the stability of droplet interface bilayer (Leptihn et al., 2013). It has also been used by Saeki et al. (2010) to visualize the residual solvent content of liposomes. They induced the burst of the water content of liposome with the addition of milliQ water into the outer aqueous phase. In this case, the osmotic pressure was balanced with the presence of glucose into the outer aqueous phase. Sugars have also been used by Karamdad et al. (2015) and Lu et al. (2015) to regulate the osmotic balance. Sucrose was added into the inner aqueous phase and glucose into the outer aqueous phase. However, the addition of glucose into the liposome environment may modify the lipid bilayer properties as glucose has been reported to interact with lipid head groups through hydrogen bound (Wolkers et al., 2004; Zhang et al., 2016). This may increase the bilayer stability but may also interfere with the biophysical experiments using these liposomes as biomimetic models. The presence of sugar to produce biomimetic models should therefore be avoided as much as possible.

To overcome the bursting problem without modifiying the composition of the phases, a second approach was explored using the droplet emulsion transfer principle. With this approach the w/o emulsion, produced at the first channel junction of the chip, formed new dispersed systems at the second channel junction. These new dispersed systems were either octanol droplets surrounded by a monolayer of lipids coming from W2 or true liposomes where a W1 droplet surrounded by a second monolayer of lipids coming from W2 (figure 22). In the last case, a thin octanol layer is observed between the two lipid monolayers.

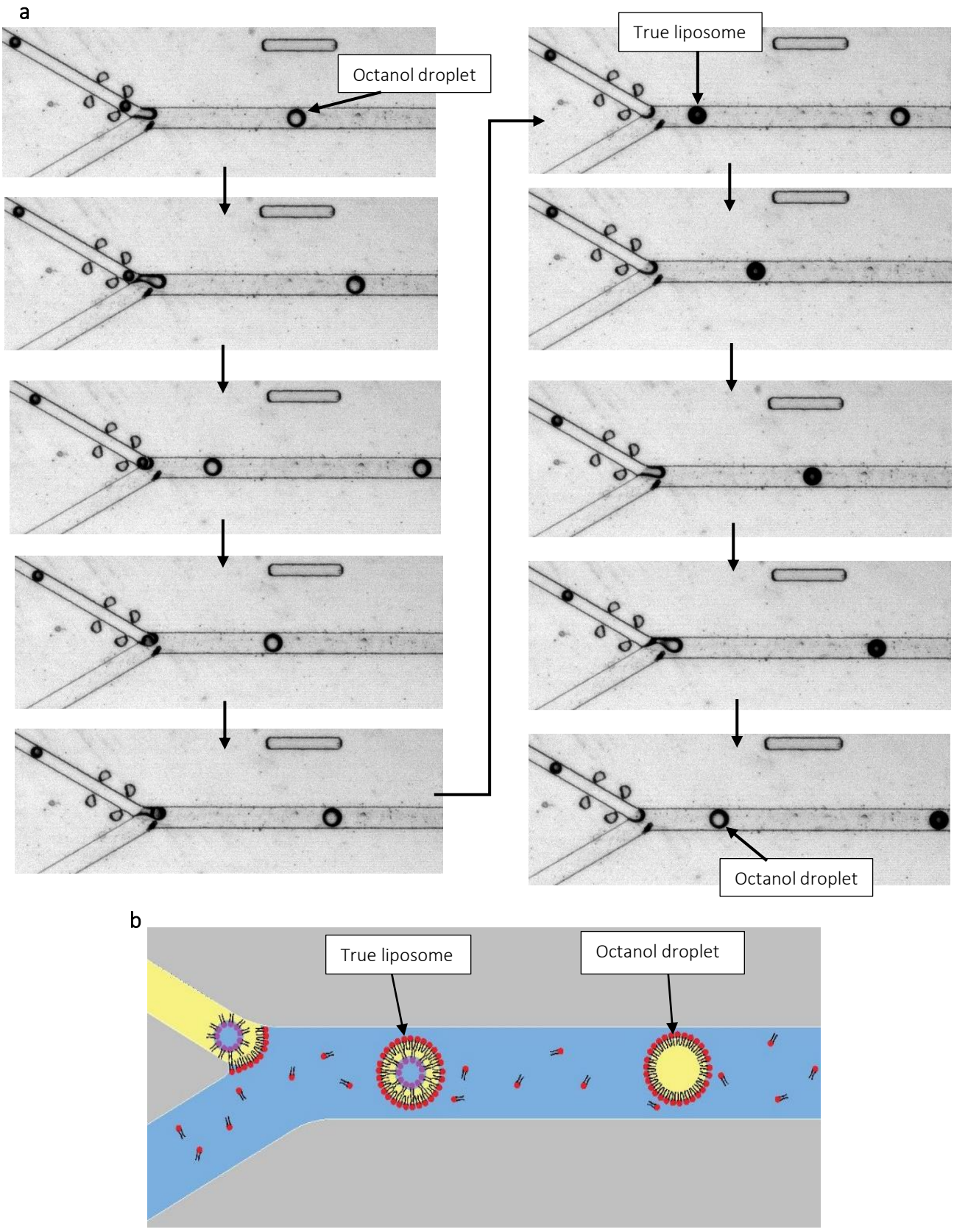

Figure 22 (a) Sequence of bright-field images and (b) schematic of liposome formation with the droplet emulsion transfer. Each image is separated with a time of 6 ms and were obtained with Q_{W1}= 0.08 µL.min^{-1} ,Q_O = 1.02 µL.min^{-1} and Q_{W2}= 20.45 µL.min^{-1}

Even though liposomes were effectively produced with this method, some of the W1 droplets formed at the first channel junction of the chip burst when arriving at the second channel junction instead of producing a liposome (figure 23).

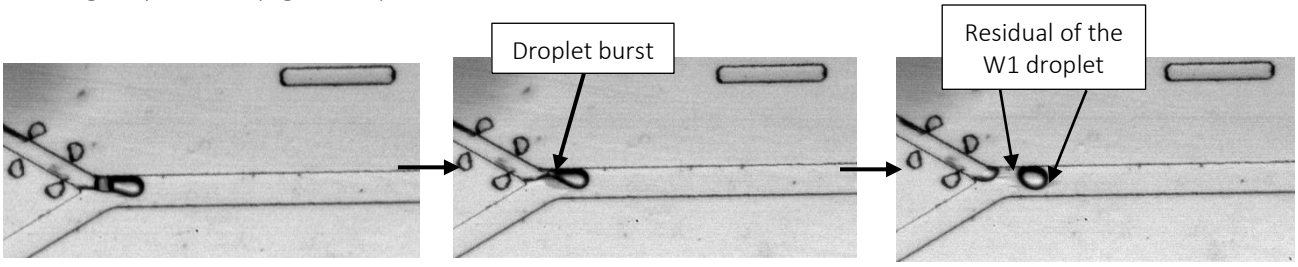

Figure 23 Image of a droplet burst with the droplet emulsion transfer principle (scale bar = 416 µm)

6.3. Analysis of liposome production

To explore the stability of the liposome production with the droplet emulsion transfer, eight situations with different flow rates of the W1, octanol and W2 phases were studied. For each situation, the median diameter of arriving W1 droplets and formed liposomes was measured (see section 7.4.). The success rate of liposome formation was also calculated as the ratio between the number of true liposomes formed and the number of W1 droplets observed. The flow rates and measurements of each situation are presented in table 4.

Table 4 Flow rates of W1 (QW1), octanol (QO) and W2 (QW2) phases, median diameters of W1 droplets and liposomes and success rate of liposome formation of eight different situation using the droplet emulsion transfer. The error on flow rates correspond to the sum of errors made on velocity and channel size measurements. The error on median diameters correspond to the error made during the image processing, sets at the size of two pixels. The number n correspond to the number of droplet measured.

Qw1 (µL . min^{-1})	Qo (µL . min^{-1})	Qw2 (µL . min^{-1})	Median diameter W1 droplets (µm)	Median diameter liposomes* (µm)	Success rate (%)
0.07 ± 0.006	0.86 ± 0.08	16.61 ± 1.49	59.49 ± 7.24 (n=57)	96.98 ± 7.24 (n=245)	18%
0.06 ± 0.008	1.19 ± 0.15	19.13 ± 2.49	61.17 ± 7.24 (n=39)	93.07 ± 7.24 (n=349)	59%
0.07 ± 0.01	1.10 ± 0.17	20.45 ± 3.07	62.76 ± 7.24 (n=36)	92.09 ± 7.24 (n=334)	37%
0.08 ± 0.01	1.02 ± 0.14	18.59 ± 2.60	65.12 ± 7.24 (n=53)	94.78 ± 7.24 (n=309)	21%
0.12 ± 0.008	0.96 ± 0.07	7.80 ± 0.55	67.15 ± 7.24 (n=69)	111.20 ± 7.24 (n=182)	0%
0.08 ± 0.008	1.25 ± 0.13	6.11 ± 0.61	63.15 ± 7.24 (n=45)	100.19 ± 7.24 (n=276)	33%
0.05 ± 0.006	1.46 ± 0.16	5.09 ± 0.56	59.12 ± 7.24 (n=35)	98.08 ± 7.24 (n=271)	58%
0.18 ± 0.01	0.60 ± 0.05	4.75 ± 0.38	75.75 ± 7.24	95.34 ± 7.24	0%

*the term “liposomes” concern both octanol droplets and true liposomes as the precise detection of true liposome has not been achieved with the matlab script yet

The diameter distribution of one of the eight situation is represented in figure 24 a for W1 droplets and figure 24 b for liposomes. As these distribution are highly asymetric, the median value is more representative of the global droplet size than the mean value which is sensitve to extreme values.

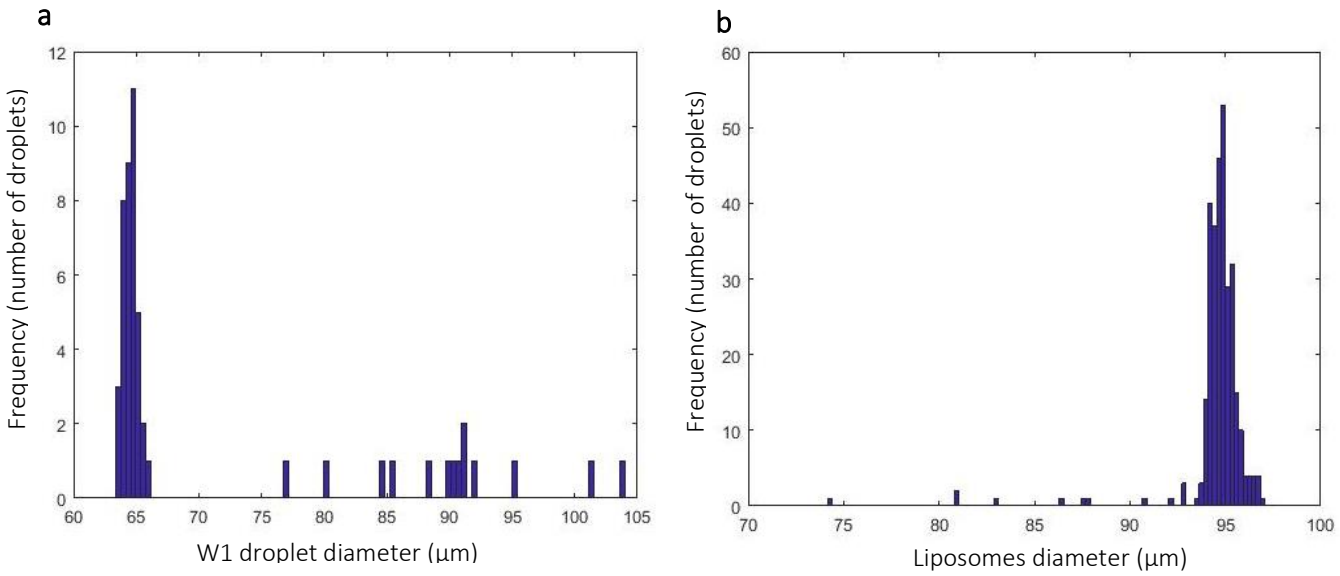

Figure 24 Example of size distribution of (a) W1 droplet (n=53) and (b) liposomes (n=306). The measurement were obtained with Q_{W1}= 0.08 µL.min^{-1} ,Q_O = 1.02 µL.min^{-1} and Q_{W2}= 20.45 µL.min^{-1}

Depending on the flow rates, the size of the produced liposomes ranges from 92 to 111 µm, with a maximum success rate of liposome formation of 59% . In comparison, the size of a plant cell is from 30 to 100 µm long and from 10 to 25 µm wide (Taiz et al., 2015). The size of the liposomes is therefore a bit larger than the plant cell size. However, the formed liposomes still contains some residual octanol (figure 25). The volume of residual octanol is supposed to be the volume of the liposomes minus the volume of the W1 droplet. This gives an average octanol volume of 338 ± 50 pL for the six situations that produced liposomes which is almost three times the average volume of the W1 droplets of 124± 14 pL. The elimination of the residual octanol is therefore required and may produce liposomes with a size closer to the W1 droplets size which ranges from 59 to 76 µm, close to the plant cell size.

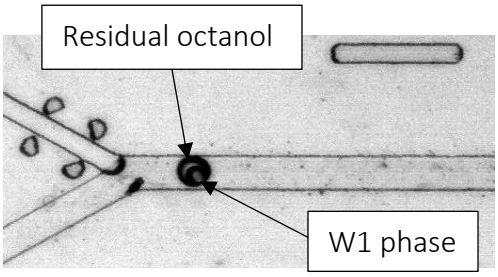

Figure 25 Image illustrating the presence of a residual octanol pocket into the liposome (scale bar = 416 µm).

To visualize if any microfluidic parameter has an impact on the success rate of the formation of a liposome, flow rate ratios between the W1 and the octanol phase (ϕ_{W1O}), the W1 and the W2 phase (ϕ_{W1W2}) and the W1/o emulsion and the W2 phase (ϕ_{WoW2}) were calculated. The median volume of the W1 droplet (V_{W1}), the median volume of the liposomes (V_{W1O}) and their ratio (V_{W1}/V_{W1O}) were also measured. The correlation between each variables was then calculated using RStudio software. The correlation matrix obtained is shown in table 5.

Table 5 Correlation matrix of the studied microfluidic parameters based on measurement taken on eight videos

	ϕ_{W1OW2}	ϕ_{W1O}	ϕ_{W1W2}	V_{W1}/V_{W1O}	V_{W1}	V_{W1O}	Success
ϕ_{W1OW2}	1	0.04	0.40	-0.11	0.07	0.30	0.17
ϕ_{W1O}	0.04	1	0.93	0.86	0.97	0.08	-0.73
ϕ_{W1W2}	0.40	0.93	1	0.74	0.92	0.20	-0.59
V_{W1}/V_{W1O}	-0.11	0.86	0.74	1	0.86	-0.40	-0.40
V_{W1}	0.07	0.97	0.92	0.86	1	0.13	-0.70
V_{W1O}	0.30	0.08	0.20	-0.40	0.13	1	-0.48
Success	0.17	-0.73	-0.59	-0.40	-0.70	-0.48	1

The results showed an influence of ϕ_{W1O} and V_{W1} on the success rate of liposome formation. Both parameters affect negatively the success rate as illustrated by their important negative correlation of -0.72 for ϕ_{W1O} and -0.71 for V_{W1}.

The effect of these variables might be explained by the diminution of the octanol layer surrounding the W1 droplet at the junction when the droplet size increases. This octanol layer is important to allow the stable assembly of the two lipid leaflets of the liposome that are both required to stabilize the liposome efficiently. At higher ϕ_{W1O}, higher W1 droplet size is observed, as illustrated by the high positive correlation of 0.97 between ϕ_{W1O} and Vol_W1, reducing the thickness of the octanol layer. When the W1 droplet comes to the second junction, only the inner leaflet is already formed but the outer leaflet still need to be assembled. Nevertheless, if the octanol layer is too thin, the two aqueous phases are not separated enough to allow the assembly of the outer leaflet before the two phases merge.

Moreover, the non-confinement of W1 droplets into the meander channel enable the fusion of successive W1 droplets into the channel before reaching the second channel junction, increasing the size of the resulting W1 droplet (figure 26). This phenomenon was more present with higher value of ϕ_{W1O} as the increase of ϕ_{W1O} reduces the amount of octanol separating two W1 droplets. If a W1 droplet has a slightly lower velocity, due to a slightly bigger size, it is caught up more easily by the following droplets as the

distance separating them is shorter. The size of the newly formed droplet is therefore twice bigger than the original W1 droplet and when arriving at the second channel junction, this bigger droplet directly bursts into the W2 phase.

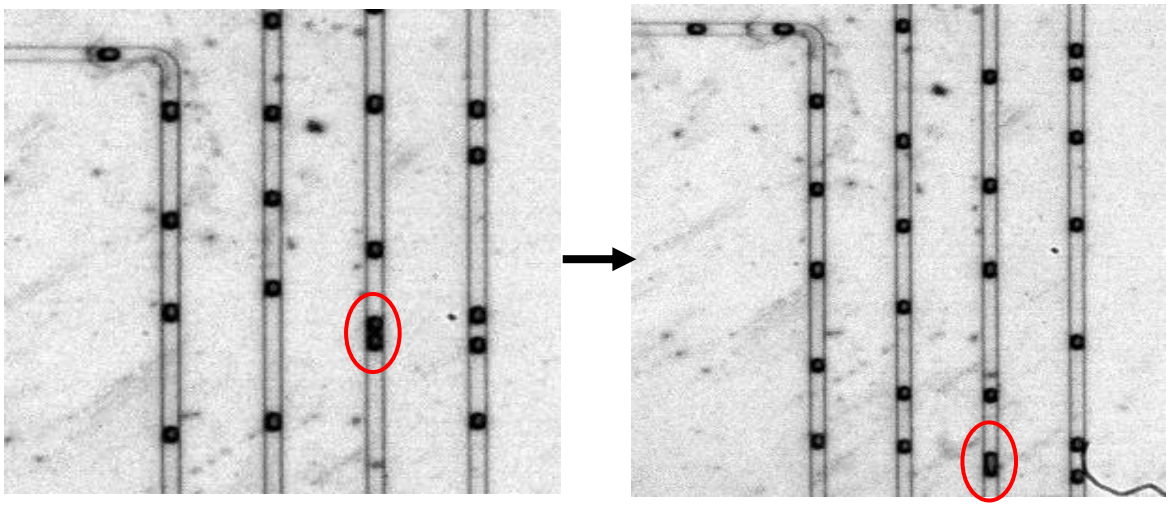

Figure 26 Image of the fusion of two W1 droplets into the meander channel

However, the correlation between the success rate of forming liposomes and the two previously mentioned variables is only of -0.72 for ϕ_{W1O} and -0.71 for Vol_W1. As the two variables are highly correlated, they give an account of a similar information. Therefore, other factors should be related with this success rate such as the osmotic pressure or the synchronization between W1 droplet arrival and lipid monolayer formation at the interface between the octanol and the W2 phases at the second channel junction.

The osmotic pressure may have impacted the success by inducing droplet burst in the same way than in the spontaneous transfer across laminar interface approach.

Concerning the synchronization between W1 droplet arrival and the lipid monolayer formation at the second channel junction, it was observed during the image analysis that a correct timing for the W1 droplet arrival is a condition for a successful liposome formation.

In a successful liposome formation, the W1 droplet comes when the w/o droplet is still growing (figure 27 a). In opposite, if the W1 droplet arrives when the pinching preceding the liberation of the w/o droplet occurs, the W1 droplet bursts into the W2 phase (figure 27 b). The pinching and the liberation of the octanol droplet may destabilize the interface between the W1 droplet and the W2 phase and decrease considerably the amount of octanol separating both aqueous phases. As a consequence, the stable lipid bilayer is not formed when these phases are in contact inducing the merge of the W1 droplet with the W2 phase.

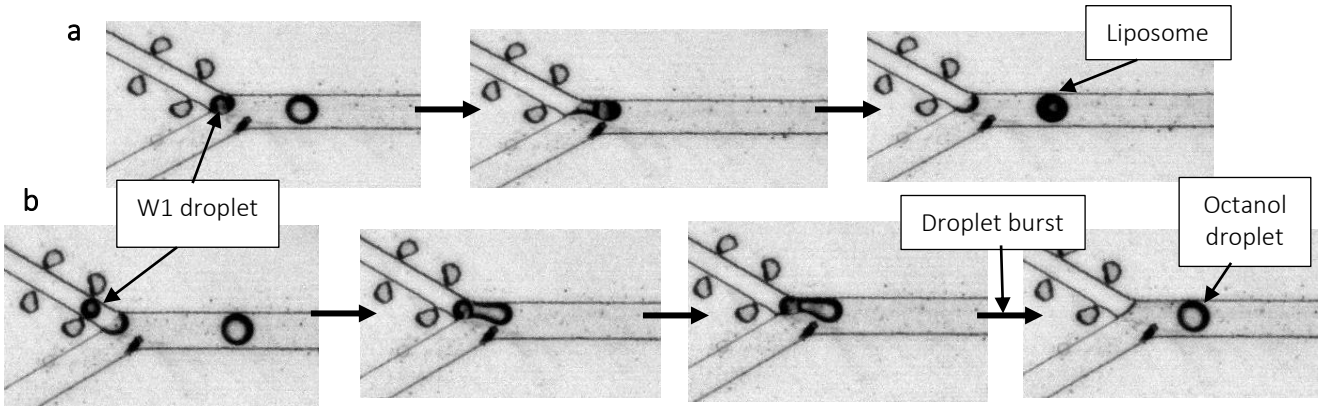

Figure 27 Comparison of the moment when a W1 droplet arrives in (a) a successful liposome formation and (b) a W1 droplet burst

In addition, the non-confinement of the W1 droplets induces a variability in the synchronization between the W1 droplet arrival and the liberation of the w/o droplet. Indeed, as the velocity of the W1 droplets may vary, the distance (i.e. the amount of octanol) separating two droplets may vary as well. As each w/o droplet generated at the second channel junction contains almost the same volume, the variation of the volume separating two W1 droplets induces a variation in the number of w/o droplets generated between the arrivals of successive W1 droplets. This may also modify the synchronization between the W1 droplet arrival and the liberation of the liposome, producing the arrival of W1 droplet when the pinching and the liberation of a liposome occurs.

6.4. Comparison of the two approaches and potential improvements

Two approaches has been tested to produce liposomes in this work and only one using the droplet emulsion transfer method has led to the production of liposomes. Nevertheless the liposomes formed still contain some residual octanol (figure 25) and the best yield of the conversion of W1 droplets into liposomes was 59 %. Besides, with the droplet emulsion transfer, octanol droplets are also formed alongside the liposomes and should be eliminated to perform experiment on formed liposomes.

Some modifications are therefore conceivable to improve the presented methodologies to produce liposomes.

Even though the transfer across laminar interface approach was not able to produce liposomes in this work, some leads can be explored to produce liposome with an easy way to separate the organic solvent from the W2 phase containing liposomes. Indeed, with the partial PVA treatment, the octanol phase formed a laminar interface with the W2 phase, allowing an easy separation of both phases with a simple Y-junction.

To get liposomes with this approach, the transfer across the laminar interface could be forced with a triangular post before the droplet bursts as realized in the device of Matosevic et al. (2011) (figure 28). The W1 droplet stability may also be increased by the addition of glucose into the W2 phase to balance the osmotic pressure across the lipid bilayer as discussed earlier. Finally the impact of the difference of viscosity between the octanol and the W2 phases on the droplet stability could be assessed with the use of less viscous organic phase such as a mixture of chloroform and hexane (38:62, v/v) used by Deng, Wang, et al. (2016) to assemble polymersomes.

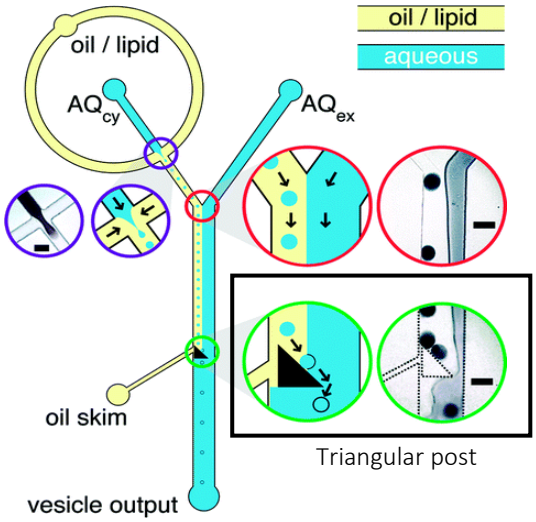

Figure 28 Device used by Matosevic et al. (2011) to produce liposomes with a triangular post to force the droplet to cross the laminar interface (adapted from Matosevic et al. (2011))

Concerning the droplet emulsion transfer, the droplet confinement into the meander channel is probably the first improvement to do. The non-confinement of droplets induced indeed the burst of W1 droplets due to the merge of W1 droplets into the meander as well as a variation of the synchronization between the W1 droplet arrival and the liberation of the w/o droplet at the second junction. The width of the meander should therefore be decreased. The decrease of channel width will increase the chip resistance and to avoid leakage at inlets, the length of this channel should also be shortened. This will diminish the time given to the lipids to form the inner leaflet but it should still be enough as lipid bilayer has been reported to be formed more rapidly when the lipids are dispersed into the aqueous phase (Leptihn et al., 2013).

If there is still many W1 droplets that burst after the modification of the meander channel, the use of sugar to regulate the osmotic pressure and increase the droplet stability could also be considered.

Along with the droplet stability, the elimination of the residual octanol observed into the liposome is also important. To achieve this step, a first measure could be the decrease of the size of the liposomes

generated at the second junction to decrease the proportion of octanol phase composing the true liposomes. This could be achieved by adjusting the ratio between the width of the channel bringing the w/o emulsion (table 3, channel 3) and the width of the channel containing the w/o/w double emulsion (table 3, channel 5). In a T-junction, van Steijn et al. (2010) have demonstrated that, for a given flow rate, this ratio is directly correlated with the size of the droplet generated. Therefore, to decrease the size of the w/o droplet, the ratio should decrease by decreasing the width of the channel 5 right after the second channel junction of the chip.

In addition, the elimination of octanol from the liposome may also occur with a spontaneous dewetting process as observed in the octanol-assisted liposome assembly developed by Deshpande et al. (2016) (figure 29). This phenomenon was not observed in the present work as the liposome did not stayed enough time into the chip. A modification of the channel width and/or the addition of outlet channel to take out some W2 phase after the liposome formation and decrease the fluid velocity should be envisaged to increase the time spent by liposomes into the chip.

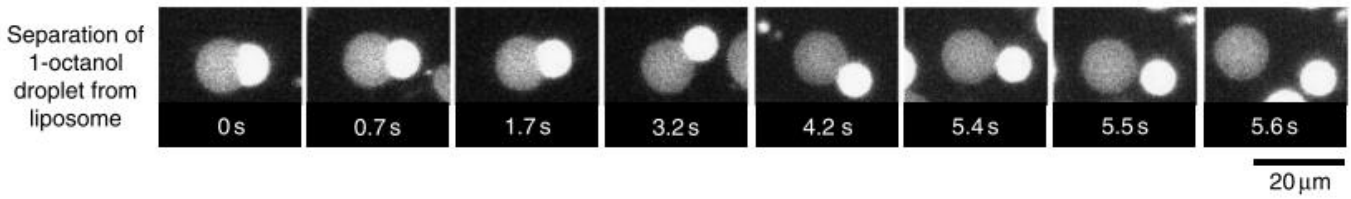

Figure 29 Temporal-resolution sequences showing the separation of the 1-octanol droplet from the liposome (reprinted from Deshpande et al. (2016))

Nevertheless, the coexistence of octanol droplets with liposomes will require a separation step to collect liposomes apart from the octanol droplets. The purification of liposomes could be partially achieved with a density based separation developed by Deshpande et al. (2018). The Microfluidics Lab is also developing a microfluidic device to sort droplets using valves that could be helpful to achieve this separation step.

7. Conclusion

In the present work, a microfluidic device has been developed to produce liposomes with a size around 100 µm, slightly larger than plant cells.

The design of the developed chip contains two channel junctions to assemble the two leaflets of the liposome one after the other. In this way, the microfluidic design is expected to allow the production of liposomes with an asymmetric lipid composition between leaflets.

The microfluidic chip was fabricated with PDMS using soft lithography. Before being able to produce liposomes, some channels of the chip have to undergo a hydrophilic modification which is performed using PVA. This modification is a critical step to produce a functional microfluidic device as it has to target the channel that required to be hydrophilic only. Furthermore, to avoid PVA clogs into the chip and get an efficient PVA treatment, the concentration of the PVA solution and the time between the plasma exposure of the PDMS chip and the treatment must be adjusted.

Two approaches were considered to produce liposomes with the developed device: the spontaneous transfer across laminar interface and the droplet emulsion transfer. With the experimental conditions chosen, only the second approach led to the production of liposomes that still contain some residual octanol.

In conclusion, this master thesis offers guidelines to develop a microfluidic device able to produce liposomes.

Nevertheless, the optimization of channel width and geometry and/or the addition of sugars into the aqueous phases to balance the osmotic pressure are suggestions to improve the presented methodology.

When stable liposomes with little residual solvent are achieved, the assessment of their unilamellarity and their potential asymmetry will have to be conducted. The unilamellarity assessment may be realized using the pore-forming protein α-haemolysin (Matosevic et al., 2013; Lu et al., 2015; Karamdad et al., 2016). The ability to produce asymmetric liposomes could be performed with fluorescence quenching assay with the addition of fluorescent lipids such as NBD-PE into either the W1 or the W2 phase and use dithionite as quencher (Matosevic et al., 2013).

After these preliminary experiments, more complex asymmetric models closer to the plant plasma membrane could be produced with commercially available plant lipids such as PLPC, GluCer and sitosterol

(Deleu et al., 2014). To be consistent with the model proposed by Mamode Cassim et al. (2019), GluCer should be exclusively located into the outer leaflet, which should be enriched with sitosterol. To achieve such model, the W1 phase would contain PLPC and sitosterol and the W2 would contain PLPC, GluCer and sitosterol in a higher amount than W1.

These new plant biomimetic models will provide new perspectives for the fundamental understanding of the structural organization of plant PM and its interaction with bioactive molecules such as elicitors. In the agronomic context, this can help to develop new plant protection product more ecofriendly and less hazardous for human health.

References

Anna S.L., 2016. Droplets and Bubbles in Microfluidic Devices. *Annu. Rev. Fluid Mech.* **48**(1), 285–309.

Basu D. & Haswell E.S., 2017. Plant mechanosensitive ion channels: an ocean of possibilities. *Curr. Opin. Plant Biol.* **40**, 43–48.

Buchoux S., Lai-Kee-Him J., Garnier M., Tsan P., Besson F., Brisson A. & Dufourc E.J., 2008. Surfactin-Triggered Small Vesicle Formation of Negatively Charged Membranes: A Novel Membrane-Lysis Mechanism. *Biophys. J.* **95**(8), 3840–3849.

Buscema M., Deyhle H., Pfohl T., Zumbuehl A. & Müller B., 2019. Spatially resolved small-angle X-ray scattering for characterizing mechanoresponsive liposomes using microfluidics. *Mater. Today Bio* **1**, 100003.

Cacas J.-L., Buré C., Grosjean K., Gerbeau-Pissot P., Lherminier J., Rombouts Y., Maes E., Bossard C., Gronnier J., Furt F., Fouillen L., Germain V., Bayer E., Cluzet S., Robert F., Schmitter J.-M., Deleu M., Lins L., Simon-Plas F. & Mongrand S., 2016. Revisiting Plant Plasma Membrane Lipids in Tobacco: A Focus on Sphingolipids. *Plant Physiol.* **170**(1), 367–84.

Cacas J.L., Furt F., Le Guédard M., Schmitter J.M., Buré C., Gerbeau-Pissot P., Moreau P., Bessoule J.J., Simon-Plas F. & Mongrand S., 2012. Lipids of plant membrane rafts. *Prog. Lipid Res.*

Cao X., Wang A., Wang C., Mao D., Lu M., Cui Y. & Jiao R., 2010. Surfactin induces apoptosis in human breast cancer MCF-7 cells through a ROS/JNK-mediated mitochondrial/caspase pathway. *Chem. Biol. Interact.* **183**(3), 357–362.

Carrillo C., Teruel J.A., Aranda F.J. & Ortiz A., 2003. Molecular mechanism of membrane permeabilization by the peptide antibiotic surfactin. *Biochim. Biophys. Acta - Biomembr.* **1611**(1–2), 91–97.

Carugo D., Bottaro E., Owen J., Stride E. & Nastruzzi C., 2016. Liposome production by microfluidics: potential and limiting factors. *Sci. Rep.* **6**(1), 25876.

Cheng H.-T. & London E., 2011. Preparation and Properties of Asymmetric Large Unilamellar Vesicles: Interleaflet Coupling in Asymmetric Vesicles Is Dependent on Temperature but Not Curvature. *Biophys. J.* **100**(11), 2671–2678.

Cheng H.-T., Megha & London E., 2009. Preparation and properties of asymmetric vesicles that mimic cell membranes: effect upon lipid raft formation and transmembrane helix orientation. *J. Biol. Chem.* **284**(10), 6079–92.

Chiantia S. & London E., 2012. Acyl Chain Length and Saturation Modulate Interleaflet Coupling in

Asymmetric Bilayers: Effects on Dynamics and Structural Order. *Biophys. J.* **103**(11), 2311–2319.

Cui P. & Wang S., 2018. Application of microfluidic chip technology in pharmaceutical analysis: A review. *J. Pharm. Anal.*

D'Auria L., Deleu M., Dufour S., Mingeot-Leclercq M.-P. & Tyteca D., 2013. Surfactins modulate the lateral organization of fluorescent membrane polar lipids: A new tool to study drug:membrane interaction and assessment of the role of cholesterol and drug acyl chain length. *Biochim. Biophys. Acta - Biomembr.* **1828**(9), 2064–2073.

Deleu M., Bouffioux O., Razafindralambo H., Paquot M., Hbid C., Thonart P., Jacques P. & Brasseur R., 2003. Interaction of surfactin with membranes: A computational approach. *Langmuir* **19**(8), 3377–3385.

Deleu M., Crowet J.M., Nasir M.N. & Lins L., 2014. Complementary biophysical tools to investigate lipid specificity in the interaction between bioactive molecules and the plasma membrane: A review. *Biochim. Biophys. Acta - Biomembr.* **1838**(12), 3171–3190.

Deleu M., Lorent J., Lins L., Brasseur R., Braun N., El Kirat K., Nylander T., Dufrêne Y.F. & Mingeot-Leclercq M.-P., 2013. Effects of surfactin on membrane models displaying lipid phase separation. *Biochim. Biophys. Acta - Biomembr.* **1828**(2), 801–815.

Deng N.-N., Yelleswarapu M. & Huck W.T.S., 2016. Monodisperse Uni- and Multicompartment Liposomes. *J. Am. Chem. Soc.* **138**(24), 7584–7591.

Deng N.N., Wang W., Ju X.J., Xie R. & Chu L.Y., 2016. Spontaneous transfer of droplets across microfluidic laminar interfaces. *Lab Chip* **16**(22), 4326–4332.

Deshpande S., Caspi Y., Meijering A.E.C.C. & Dekker C., 2016. Octanol-assisted liposome assembly on chip. *Nat. Commun.* **7**, 1–9.

Deshpande S. & Dekker C., 2018. On-chip microfluidic production of cell-sized liposomes. *Nat. Protoc.* **13**(5), 856–874.

Dufour S., Deleu M., Nott K., Wathelet B., Thonart P. & Paquot M., 2005. Hemolytic activity of new linear surfactin analogs in relation to their physico-chemical properties. *Biochim. Biophys. Acta - Gen. Subj.* **1726**(1), 87–95.

Eeman M. & Deleu M., 2010. From biological membranes to biomimetic model membranes. *Biotechnol. Agron. Soc. Environ.* **14**(4), 719–736.

Elani Y., Purushothaman S., Booth P.J., Seddon J.M., Brooks N.J., Law R. V. & Ces O., 2015. Measurements of the effect of membrane asymmetry on the mechanical properties of lipid bilayers. *Chem. Commun.*

51(32), 6976–6979.

Falardeau J., Wise C., Novitsky L. & Avis T.J., 2013. Ecological and Mechanistic Insights Into the Direct and Indirect Antimicrobial Properties of Bacillus subtilis Lipopeptides on Plant Pathogens. *J. Chem. Ecol.* **39**(7), 869–878.

Fan H.Y., Nazari M., Raval G., Khan Z., Patel H. & Heerklotz H., 2014. Utilizing zeta potential measurements to study the effective charge, membrane partitioning, and membrane permeation of the lipopeptide surfactin. *Biochim. Biophys. Acta - Biomembr.* **1838**(9), 2306–2312.

Fezoua-Boubegtiten Z., Hastoy B., Scotti P., Milochau A., Bathany K., Desbat B., Castano S., Oda R. & Lang J., 2019. The transmembrane domain of the SNARE protein VAMP2 is highly sensitive to its lipid environment. *Biochim. Biophys. Acta - Biomembr.* **1861**(3), 670–676.

Fiedler S. & Heerklotz H., 2015. Vesicle Leakage Reflects the Target Selectivity of Antimicrobial Lipopeptides from Bacillus subtilis. *Biophys. J.* **109**(10), 2079–2089.

Fira D., Dimkić I., Berić T., Lozo J. & Stanković S., 2018. Biological control of plant pathogens by Bacillus species. *J. Biotechnol.* **285**, 44–55.

Francius G., Dufour S., Deleu M., Paquot M., Mingeot-Leclercq M.-P. & Dufrêne Y.F., 2008. Nanoscale membrane activity of surfactins: Influence of geometry, charge and hydrophobicity. *Biochim. Biophys. Acta - Biomembr.* **1778**(10), 2058–2068.

Furt F., Simon-Plas F. & Mongrand S., 2011. Lipids of the Plant Plasma Membrane. *In*: *The Plant Plasma Membrane*. Springer, Berlin, Heidelberg, 3–30.

Gao F., Su Z.-G., Wang P. & Ma G.-H., 2009. Double Emulsion Templated Microcapsules with Single Hollow Cavities and Thickness-Controllable Shells. *Langmuir* **25**(6), 3832–3838.

Grau A., Gómez Fernández J.C., Peypoux F. & Ortiz A., 1999. A study on the interactions of surfactin with phospholipid vesicles. *Biochim. Biophys. Acta - Biomembr.* **1418**(2), 307–319.

Gronnier J., Gerbeau-Pissot P., Germain V., Mongrand S. & Simon-Plas F., 2018. Divide and Rule: Plant Plasma Membrane Organization. *Trends Plant Sci.* **23**(10), 899–917.

Guillot P., Panizza P., Salmon J.-B., Joanicot M., Colin A., Bruneau C.-H. & Colin T., 2006. Viscosimeter on a Microfluidic Chip. *Langmuir* **22**(14), 6438–6445.

Guo D., Venkatramesh M. & Nes W.D., 1995. Developmental regulation of sterol biosynthesis inZea mays. *Lipids* **30**(3), 203–219.

Heerklotz H. & Seelig J., 2000. Titration calorimetry of surfactant–membrane partitioning and membrane

solubilization. *Biochim. Biophys. Acta - Biomembr.* **1508**(1–2), 69–85.

Heerklotz H. & Seelig J., 2001. Detergent-like action of the antibiotic peptide surfactin on lipid membranes. *Biophys. J.* **81**(3), 1547–54.

Heerklotz H. & Seelig J., 2007. Leakage and lysis of lipid membranes induced by the lipopeptide surfactin. *Eur. Biophys. J.* **36**(4–5), 305–314.

Heerklotz H., Wieprecht T. & Seelig J., 2004. Membrane Perturbation by the Lipopeptide Surfactin and Detergents as Studied by Deuterium NMR.

Henry G., Deleu M., Jourdan E., Thonart P. & Ongena M., 2011. The bacterial lipopeptide surfactin targets the lipid fraction of the plant plasma membrane to trigger immune-related defence responses. *Cell. Microbiol.* **13**(11), 1824–1837.

Hovakeemian S.G., Liu R., Gellman S.H. & Heerklotz H., 2015. Correlating antimicrobial activity and model membrane leakage induced by nylon-3 polymers and detergents. *Soft Matter* **11**(34), 6840–6851.

Huang X., Lu Z., Zhao H., Bie X., Lü F. & Yang S., 2006. Antiviral Activity of Antimicrobial Lipopeptide from Bacillus subtilis fmbj Against Pseudorabies Virus, Porcine Parvovirus, Newcastle Disease Virus and Infectious Bursal Disease Virus in Vitro. *Int. J. Pept. Res. Ther.* **12**(4), 373–377.

Huang Z. & London E., 2013. Effect of Cyclodextrin and Membrane Lipid Structure upon Cyclodextrin–Lipid Interaction. *Langmuir* **29**(47), 14631–14638.

Hussain N.F., Siegel A.P., Ge Y., Jordan R. & Naumann C.A., 2013. Bilayer Asymmetry Influences Integrin Sequestering in Raft-Mimicking Lipid Mixtures. *Biophys. J.* **104**(10), 2212–2221.

Jahn A., Stavis S.M., Hong J.S., Vreeland W.N., DeVoe D.L. & Gaitan M., 2010. Microfluidic Mixing and the Formation of Nanoscale Lipid Vesicles. *ACS Nano* **4**(4), 2077–2087.

Jahn A., Vreeland W.N., DeVoe D.L., E. Locascio L. & Gaitan M., 2007. Microfluidic Directed Formation of Liposomes of Controlled Size.

Jakiela S., Makulska S., Korczyk P.M. & Garstecki P., 2011. Speed of flow of individual droplets in microfluidic channels as a function of the capillary number, volume of droplets and contrast of viscosities. *Lab Chip* **11**(21), 3603.

Jimenez-Jimenez S., Hashimoto K., Santana O., Aguirre J., Kuchitsu K. & Cárdenas L., 2019. Emerging roles of tetraspanins in plant inter-cellular and inter-kingdom communication. *Plant Signal. Behav.* **14**(4), e1581559.

Jonathan M. Crane, Volker Kiessling and & Tamm* L.K., 2005. Measuring Lipid Asymmetry in Planar

Supported Bilayers by Fluorescence Interference Contrast Microscopy.

Kamiya K., Kawano R., Osaki T., Akiyoshi K. & Takeuchi S., 2016. Cell-sized asymmetric lipid vesicles facilitate the investigation of asymmetric membranes. *Nat. Chem.* **8**(9), 881–889.

Kamiya K. & Takeuchi S., 2017. Giant liposome formation toward the synthesis of well-defined artificial cells. *J. Mater. Chem. B* **5**(30), 5911–5923.

Karamdad K., Law R. V., Seddon J.M., Brooks N.J. & Ces O., 2015. Preparation and mechanical characterisation of giant unilamellar vesicles by a microfluidic method. *Lab Chip* **15**(2), 557–562.

Karamdad K., Law R. V., Seddon J.M., Brooks N.J. & Ces O., 2016. Studying the effects of asymmetry on the bending rigidity of lipid membranes formed by microfluidics. *Chem. Commun.* **52**(30), 5277–5280.

Kei Funakoshi †,‡, Hiroaki Suzuki † and & Shoji Takeuchi* †,‡, 2007. Formation of Giant Lipid Vesiclelike Compartments from a Planar Lipid Membrane by a Pulsed Jet Flow.

Kell H., Holzwarth J.F., Boettcher C., Heenan R.K. & Vater J., 2007. Physicochemical studies of the interaction of the lipoheptapeptide surfactin with lipid bilayers of l-α-dimyristoyl phosphatidylcholine. *Biophys. Chem.* **128**(2–3), 114–124.

Kim H.S., Devarenne T.P. & Han A., 2018. Microfluidic systems for microalgal biotechnology: A review. *Algal Res.* **30**, 149–161.

Kracht M., Rokos H., Özel M., Kowall M., Pauli G. & Vater J., 1999. Antiviral and Hemolytic Activities of Surfactin Isoforms and Their Methyl Ester Derivatives. *J. Antibiot. (Tokyo).* **52**(7), 613–619.

Leptihn S., Castell O.K., Cronin B., Lee E., Gross L.C.M., Marshall D.P., Thompson J.R., Holden M. & Wallace M.I., 2013. Constructing droplet interface bilayers from the contact of aqueous droplets in oil.

Lichtenberg D., Goñi F.M. & Heerklotz H., 2005. Detergent-resistant membranes should not be identified with membrane rafts. *Trends Biochem. Sci.* **30**(8), 430–436.

Lin Q. & London E., 2014a. The influence of natural lipid asymmetry upon the conformation of a membrane-inserted protein (perfringolysin O). *J. Biol. Chem.* **289**(9), 5467–78.

Lin Q. & London E., 2014b. Preparation of Artificial Plasma Membrane Mimicking Vesicles with Lipid Asymmetry. *PLoS One* **9**(1), e87903.

Liu X., Huang W. & Wang E., 2005. An electrochemical study on the interaction of surfactin with a supported bilayer lipid membrane on a glassy carbon electrode. *J. Electroanal. Chem.* **577**(2), 349–354.

Liu Z.-M., Yang Y., Du Y. & Pang Y., 2017. Advances in Droplet-Based Microfluidic Technology and Its Applications. *Chinese J. Anal. Chem.* **45**(2), 282–296.

Lu L., Schertzer J.W. & Chiarot P.R., 2015. Continuous microfluidic fabrication of synthetic asymmetric vesicles. *Lab Chip* **15**(17), 3591–3599.

Maget-Dana R. & Ptak M., 1992. Interfacial properties of surfactin. *J. Colloid Interface Sci.* **153**(1), 285–291.

Mamode Cassim A., Gouguet P., Gronnier J., Laurent N., Germain V., Grison M., Boutté Y., Gerbeau-Pissot P., Simon-Plas F. & Mongrand S., 2019. Plant lipids: Key players of plasma membrane organization and function. *Prog. Lipid Res.* **73**, 1–27.

Marques M.P. & Szita N., 2017. Bioprocess microfluidics: applying microfluidic devices for bioprocessing. *Curr. Opin. Chem. Eng.* **18**, 61–68.

Matosevic S. & Paegel B.M., 2011. Stepwise Synthesis of Giant Unilamellar Vesicles on a Microfluidic Assembly Line.

Matosevic S. & Paegel B.M., 2013. Layer-by-layer cell membrane assembly. *Nat. Chem.* **5**(11), 958–963.

Mazutis L., Gilbert J., Ung W.L., Weitz D.A., Griffiths A.D. & Heyman J.A., 2013. Single-cell analysis and sorting using droplet-based microfluidics. *Nat. Protoc.* **8**(5), 870–891.

Michaelson L. V., Napier J.A., Molino D. & Faure J.-D., 2016. Plant sphingolipids: Their importance in cellular organization and adaption. *Biochim. Biophys. Acta - Mol. Cell Biol. Lipids* **1861**(9), 1329–1335.

Mongrand S., Stanislas T., Bayer E.M.F., Lherminier J. & Simon-Plas F., 2010. Membrane rafts in plant cells. *Trends Plant Sci.* **15**(12), 656–663.

Nickels J.D., Smith J.C. & Cheng X., 2015. Lateral organization, bilayer asymmetry, and inter-leaflet coupling of biological membranes. *Chem. Phys. Lipids* **192**, 87–99.

Nielsen J.E., Lind T.K., Lone A., Gerelli Y., Hansen P.R., Jenssen H., Cárdenas M. & Lund R., 2019. A biophysical study of the interactions between the antimicrobial peptide indolicidin and lipid model systems. *Biochim. Biophys. Acta - Biomembr.*

Nintemann S.J., Palmgren M. & López-Marqués R.L., 2019. Catch You on the Flip Side: A Critical Review of Flippase Mutant Phenotypes. *Trends Plant Sci.*

Nyholm T.K.M., 2015. Lipid-protein interplay and lateral organization in biomembranes. *Chem. Phys. Lipids* **189**, 48–55.

Oftedal L., Myhren L., Jokela J., Gausdal G., Sivonen K., Døskeland S.O. & Herfindal L., 2012. The lipopeptide toxins anabaenolysin A and B target biological membranes in a cholesterol-dependent manner. *Biochim. Biophys. Acta - Biomembr.* **1818**(12), 3000–3009.

Ongena M. & Jacques P., 2008. Bacillus lipopeptides: versatile weapons for plant disease biocontrol. *Trends*

Microbiol. **16**(3), 115–125.

Ongena M., Jourdan E., Adam A., Paquot M., Brans A., Joris B., Arpigny J.-L. & Thonart P., 2007. Surfactin and fengycin lipopeptides of Bacillus subtilis as elicitors of induced systemic resistance in plants. *Environ. Microbiol.* **9**(4), 1084–1090.

Ōyanagi Y. & Matsumoto M., 1962. Viscosity of moderately concentrated aqueous solutions of polyvinyl alcohol. *J. Colloid Sci.* **17**(5), 426–438.

Palmgren M., Østerberg J.T., Nintemann S.J., Poulsen L.R. & López-Marqués R.L., 2019. Evolution and a revised nomenclature of P4 ATPases, a eukaryotic family of lipid flippases. *Biochim. Biophys. Acta - Biomembr.* **1861**(6), 1135–1151.

Park S.Y., Kim J.-H., Lee S.J. & Kim Y., 2013. Surfactin exhibits neuroprotective effects by inhibiting amyloid β-mediated microglial activation. *Neurotoxicology* **38**, 115–123.

Patel H., Huynh Q., Bärlehner D. & Heerklotz H., 2014. Additive and synergistic membrane permeabilization by antimicrobial (lipo)peptides and detergents. *Biophys. J.* **106**(10), 2115–25.

Pautot S., Frisken B.J. & Weitz D.A., 2003. Production of Unilamellar Vesicles Using an Inverted Emulsion. *Langmuir* **19**(7), 2870–2879.

Peetla C., Stine A. & Labhasetwar V., 2009. Biophysical interactions with model lipid membranes: applications in drug discovery and drug delivery. *Mol. Pharm.* **6**(5), 1264–76.

Pérez-García A., Romero D. & de Vicente A., 2011. Plant protection and growth stimulation by microorganisms: biotechnological applications of Bacilli in agriculture. *Curr. Opin. Biotechnol.* **22**(2), 187–193.

Pomorski T.G., Nylander T. & Cárdenas M., 2014. Model cell membranes: Discerning lipid and protein contributions in shaping the cell. *Adv. Colloid Interface Sci.* **205**, 207–220.

Razafindralambo H., Dufour S., Paquot M. & Deleu M., 2009. Thermodynamic studies of the binding interactions of surfactin analogues to lipid vesicles. *J. Therm. Anal. Calorim.* **95**(3), 817–821.

Rossy J., Ma Y. & Gaus K., 2014. The organisation of the cell membrane: do proteins rule lipids? *Curr. Opin. Chem. Biol.* **20**, 54–59.

Saeki D., Sugiura S., Kanamori T., Sato S. & Ichikawa S., 2010. Microfluidic preparation of water-in-oil-in-water emulsions with an ultra-thin oil phase layer. *Lab Chip* **10**(3), 357–362.

Salehi-Reyhani A., Ces O. & Elani Y., 2017. Artificial cell mimics as simplified models for the study of cell biology. *Exp. Biol. Med.* **242**(13), 1309–1317.

Santos V.S.V., Silveira E. & Pereira B.B., 2018. Toxicity and applications of surfactin for health and environmental biotechnology. *J. Toxicol. Environ. Heal. Part B* **21**(6–8), 382–399.

Scheler O., Postek W. & Garstecki P., 2019. Recent developments of microfluidics as a tool for biotechnology and microbiology. *Curr. Opin. Biotechnol.* **55**, 60–67.

Sebaaly C. & Greige-Gerges H., 2019. Lipid Membrane Models for Biomembrane Properties' Investigation. *Curr. Trends Futur. Dev. Membr.* 311–340.

Seddon A.M., Casey D., Law R. V., Gee A., Templer R.H. & Ces O., 2009. Drug interactions with lipid membranes. *Chem. Soc. Rev.* **38**(9), 2509.

Sheetz M.P., Singer S.J., Teng J. & Kung C., 2014. Biological membranes as bilayer couples. A molecular mechanism of drug-erythrocyte interactions. *Proc. Natl. Acad. Sci. U. S. A.* **71**(11), 4457–61.

Shen H.-H., Thomas R.K., Penfold J. & Fragneto G., 2010. Destruction and Solubilization of Supported Phospholipid Bilayers on Silica by the Biosurfactant Surfactin. *Langmuir* **26**(10), 7334–7342.

Shen H.H., Thomas R.K. & Taylor P., 2010. The location of the biosurfactant surfactin in phospholipid bilayers supported on silica using neutron reflectometry. *Langmuir* **26**(1), 320–327.

Sheppard J.D., Jumarie C., Cooper D.G. & Laprade R., 1991. Ionic channels induced by surfactin in planar lipid bilayer membranes. *Biochim. Biophys. Acta - Biomembr.* **1064**(1), 13–23.

Shi H., Nie K., Dong B., Long M., Xu H. & Liu Z., 2019. Recent progress of microfluidic reactors for biomedical applications. *Chem. Eng. J.* **361**, 635–650.

Siontorou C., Nikoleli G.-P., Nikolelis D. & Karapetis S., 2017. Artificial Lipid Membranes: Past, Present, and Future. *Membranes (Basel).* **7**(3), 38.

Spitzer C., Li F., Buono R., Roschzttardtz H., Chung T., Zhang M., Osteryoung K.W., Vierstra R.D. & Otegui M.S., 2015. The endosomal protein CHARGED MULTIVESICULAR BODY PROTEIN1 regulates the autophagic turnover of plastids in Arabidopsis. *Plant Cell* **27**(2), 391–402.

Taiz L., Zeiger E., Moller I.M. & Murphy A., 2015. *Plant physiology and development*, Sinauer Associates, 761.

Tan S.H., Nguyen N.-T., Chua Y.C. & Kang T.G., 2010. Oxygen plasma treatment for reducing hydrophobicity of a sealed polydimethylsiloxane microchannel. *Biomicrofluidics* **4**(3), 032204.

Thimon L., Peypoux F. & Michel G., 1992. Interactions of surfactin, a biosurfactant fromBacillus subtilis, with inorganic cations. *Biotechnol. Lett.* **14**(8), 713–718.

Tjellström H., Hellgren L.I., Wieslander Å. & Sandelius A.S., 2010. Lipid asymmetry in plant plasma

membranes: phosphate deficiency-induced phospholipid replacement is restricted to the cytosolic leaflet. *FASEB J.* **24**(4), 1128–1138.

Trantidou T., Elani Y., Parsons E. & Ces O., 2017. Hydrophilic surface modification of PDMS for droplet microfluidics using a simple, quick, and robust method via PVA deposition. *Microsystems Nanoeng.* **3**, 16091.

van Loo S., Stoukatch S., Kraft M. & Gilet T., 2016. Droplet formation by squeezing in a microfluidic cross-junction. *Microfluid. Nanofluidics* **20**(10), 1–12.

van Meer G., 2011. Dynamic transbilayer lipid asymmetry. *Cold Spring Harb. Perspect. Biol.* **3**(5), a004671.

van Meer G., Voelker D.R. & Feigenson G.W., 2008. Membrane lipids: where they are and how they behave. *Nat. Rev. Mol. Cell Biol.* **9**(2), 112–124.

van Steijn V., Kleijn C.R. & Kreutzer M.T., 2010. Predictive model for the size of bubbles and droplets created in microfluidic T-junctions. *Lab Chip* **10**(19), 2513.

Wolkers W.F., Oldenhof H., Tablin F. & Crowe J.H., 2004. Preservation of dried liposomes in the presence of sugar and phosphate. *Biochim. Biophys. Acta - Biomembr.* **1661**(2), 125–134.

Wu D., Luo Y., Zhou X., Dai Z. & Lin B., 2005. Multilayer poly(vinyl alcohol)-adsorbed coating on poly(dimethylsiloxane) microfluidic chips for biopolymer separation. *Electrophoresis* **26**(1), 211–218.

Xue H.-W., Chen X. & Mei Y., 2009. Function and regulation of phospholipid signalling in plants. *Biochem. J.* **421**(2), 145–56.

Yamazaki T., Owari S., Ota S., Sumiya N., Yamamoto M., Watanabe K., Nagumo T., Miyamura S. & Kawano S., 2013. Localization and evolution of septins in algae. *Plant J.* **74**(4), 605–614.

Zhang W., Falconer J.R., Baguley B.C., Shaw J.P., Kanamala M., Xu H., Wang G., Liu J. & Wu Z., 2016. Improving drug retention in liposomes by aging with the aid of glucose. *Int. J. Pharm.* **505**(1–2), 194–203.

Zhao C.X., 2013. Multiphase flow microfluidics for the production of single or multiple emulsions for drug delivery. *Adv. Drug Deliv. Rev.* **65**(11–12), 1420–1446.

Zhao H. & Lappalainen P., 2012. A simple guide to biochemical approaches for analyzing protein–lipid interactions. *Mol. Biol. Cell* **23**(15), 2823–2830.

Zhao P., Xue Y., Li X., Li J., Zhao Z., Quan C., Gao W., Zu X., Bai X. & Feng S., 2019. Fungi-derived lipopeptide antibiotics developed since 2000. *Peptides* **113**, 52–65.

Zhuang X., Wang H., Lam S.K., Gao C., Wang X., Cai Y. & Jiang L., 2013. A BAR-domain protein SH3P2, which

binds to phosphatidylinositol 3-phosphate and ATG8, regulates autophagosome formation in Arabidopsis. *Plant Cell* **25**(11), 4596–615.